Supporting Online Material for

The Buttermilk Creek Complex and the Origins of Clovis at the Debra L. Friedkin Site, Texas

Michael R. Waters,* Steven L. Forman, Thomas A. Jennings, Lee C. Nordt, Steven G. Driese, Joshua M. Feinberg, Joshua L. Keene, Jessi Halligan, Anna Lindquist, James Pierson, Charles T. Hallmark, Michael B. Collins, James E. Wiederhold

*To whom correspondence should be addressed. E-mail: mwaters@tamu.edu

Published 25 March 2011, *Science* **331**, 1599 (2011)
DOI: 10.1126/science.1201855

This PDF file includes:

Stratigraphy

Block B is located on Terrace 1. The oldest deposits in Block B (Fig. S1) are fluvial channel gravels (unit 1a) overlain by floodplain clays (unit 1b). Sediment from unit 1b yielded five luminescence ages ranging from 39,000 to 19,000 yr B.P. and contained no artifacts or faunal remains. Unit 1 was eroded and a 4 m-wide channel was created. This channel filled with multiple thin layers of sand and gravel (unit 2a) that are interbedded with clay (unit 2b). At the base of the channel are Clovis artifacts (blades, blade cores, end-thinned bifaces, a fluted preform, and other tools) and above this are later artifacts, including an Angostura point. These artifacts represent prehistoric activities that took place in and adjacent to the channel. Five luminescence ages from the clay sediments (unit 2b) range from 13,885 $\pm$ 1015 yr B.P. (UIC-2383; associated with Clovis) to 9860 $\pm$ 740 yr B.P. (UIC-2378; above the Angostura point). These sediments were truncated by later erosion and channel formation. The next sequence of deposits consists of basal gravels (unit 3a) containing a Middle Archaic Andice point (ca. 5500 to 6800 yr B.P.). This is overlain by fine-grained silt and clay sediments (units 3b, 3d, and 3f) and occasional sand lenses in small channels (units 3c and 3e). Three luminescence ages from the fine-grained sediments center around 4000 yr B.P. These deposits represent ancestral channels and floodplains of Buttermilk Creek.

The stratigraphy of Block A was described in the main text. Figure S2 shows the general landscape setting of the block excavation. Figure S3 provides a photograph showing the limestone bedrock, overlying colluvium, and floodplain clays in Block A.

The channel history of T-1 correlates with the floodplain depositional history of T-2. From ca. 35,000-40,000 to 13,200 yr B.P., the creek and floodplain aggraded. From ca. 13,200 to 12,900 yr B.P., Buttermilk Creek downcut and deposition resumed in the channel with some deposition on the floodplain. Rapid sedimentation occurs in the channel and on the floodplain at the end of the Pleistocene and during the early Holocene. This was followed by a period of slow deposition on the floodplain and channel incision during the middle Holocene, followed by renewed and rapid sedimentation during the late Holocene on both the floodplain and near the channel margin.

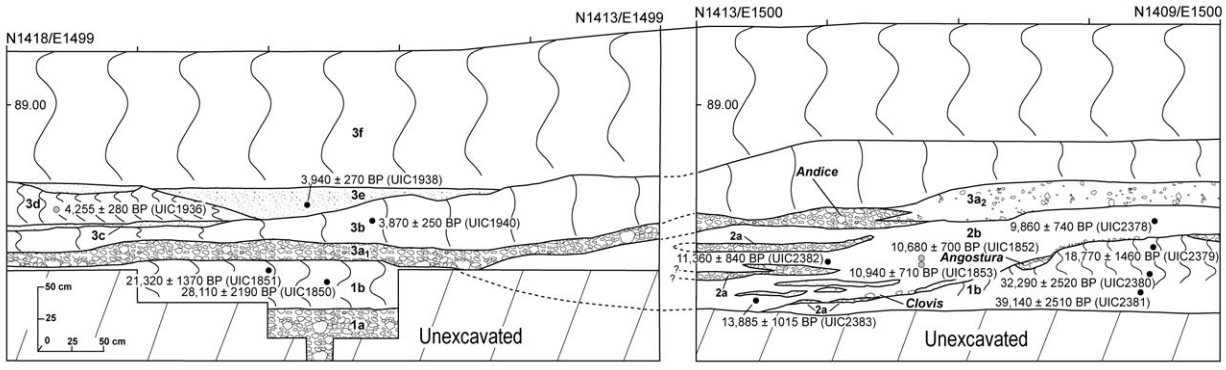

Figure S1. Stratigraphy on east wall of Block B.

Figure S2. Excavations at Block A in 2007. Buttermilk Creek flows from right to left through the trees.

Figure S3. Stratigraphy exposed in Block A in 2007. Note bedrock on the west wall (right). Light brown layer above the bedrock is the colluvium. Dark gray sediments are the floodplain deposits.

Luminescence Dating

No radiocarbon dates were obtained from these deposits because suitable datable materials were not preserved. Chronological control is provided by 63 luminescence ages (Block A, n=50; Block B, n=13).

Sediments targeted for optical dating are clay-rich distal overbank sediments. Samples for optical dating were taken by hammering a 2.6 cm interior diameter and 10-15 cm length of copper tubing into profile walls. The outermost 1 cm of sediment inside the tube was removed, leaving an unlight-exposed sediment in the center of the tube for optical dating. Optical ages were determined by multiple methods on the fine-grained polymineral or quartz fraction. Initially ages were determined on the fine grained (4-11) polymineral fraction using multiple aliquot techniques (*S1*) with initial infrared excitation followed by exposure to blue light. The fine-grained quartz separate of representative samples was isolated and dated using multiple aliquot techniques. Further, selected separates of fine-grained quartz fraction were dated using single aliquot regeneration protocols (*S2*). Note that optical ages by the three different techniques overlap at one sigma errors and are concordant with artifact chronologic control.

Luminescence dating of the sediments at the Friedkin site was possible because small amounts of silt-sized quartz and feldspar grains were present in the alluvium of the Buttermilk Creek (*S3*). This clastic material was not derived from the limestone bedrock in the drainage basin. Instead, the fine-grained particles used for dating represent eolian dust. The accumulation of wind-blown fine-grained sediments is well documented at the adjacent Gault site (*S3*) and at in other places in central Texas (*S4, S5, S6*). In turn, the fine-grained quartz fraction upon irradiation in the laboratory exhibits a prominent 110° C peak with thermoluminescence analysis, which is diagnostic of quartz (*S7*).

Multiple aliquot regeneration procedures

Multiple-aliquot regeneration (MAR) procedures with component dose normalization (*S1*) were used in this study to estimate the equivalent dose on fine-grained polymineral and quartz fraction from sediments (Table S1). Initially fine grains (4-11 micron) were extracted by suspension settling following Stokes Law after organics and carbonate were removed with soaking in H_20_2 and in HCl, respectively (cf. *S8*). Quartz extracts on the fine-grained fraction were isolated subsequently by digestion in hydrofluosilicic acid (silica saturated) for six days (*S9, S10*). Sediment plate area was 1 cm diameter. Low emissions (<200 counts/s) at or near the background counts with subsequent infrared excitation indicates a pure quartz separate. Solar resetting of aliquots prior to MAR analysis was accomplished by 8 hr illumination from a 275W General Electric Mercury Vapor Sunlamp, removing any pre-existing electrons within accessible photosensitive traps while inducing minimal dose sensitivity changes (*S11*). Luminescence was measured using a Risø Model TL/luminescence-DA-15 System containing light emitting diodes capable of either infrared (875 ± 30) or blue (470 ± 20) excitation. The resulting luminescence passes through a Hoya U-340 filter (>10% transmission >380 nm) prior to detection within the system's Thorn-EMI 9235 QA photomultiplier tube.

To compensate for laboratory-induced sensitivity changes, we used component specific normalization procedure (cf. *S1*). A normalization dose (~4 Gy β) was applied to all discs, either after the measurement of the natural luminescence signal or prior to the measurement of the dose response curve (Table S1) and the ratio of secondary to initial luminescence response was used to derive a correction factor for sensitivity changes. The efficacy of the preheat treatment (150° C for 1 hour) for the normalization dose was evaluated by comparing curve shape (trap distribution) between the natural and subsequent dose (*S12*). A similar dose response was indicated by zero or low slope (<0.1) between the luminescence for initial and secondary dose, evaluated at one-second intervals. To eliminate any contributions to the luminescence signal from electrons residing within those traps that are thermally unstable over geologic time periods, two different heating treatments were employed: first, storage at 150°C for 1 hour immediately following each laboratory irradiation (cf. *S13, S14*), and second, measurement at elevated temperature 125°C during excitation (cf. *S15*). Because the natural luminescence signal does not include any contributions from electrons residing within traps that are thermally unstable over geologic time periods, the first heating treatment is not required prior to its measurement. The temperature and duration of the first heating treatment following the subsequent normalization dose was selected from a range of temperatures (140-200°C) to mimic the charge distribution exhibited by the natural luminescence signal (Fig. S4). Success was indicated by zero or low slope (<0.1) between the luminescence for initial and secondary dose, evaluated at one-second intervals, and by a uniform equivalent dose value across the shine down curve (Fig. S5), also indicative of full solar resetting (*S12, S16*). In turn feldspar (polymineral fraction) and quartz components yielded statistically identical ages, which also indicates sediments are well solar reset because of the differential susceptibility of quartz and feldspar to solar resetting. A sequential regenerative dose of up to 165 grays was applied to each sample that exceeded the corresponding natural luminescence and this dose response was unsaturated (Fig. S5). Equivalent dose was calculated for at least the first 50 seconds of excitation, dependent on background counts, as a weighted mean (Table S1).

We used laboratory procedures that access the light sensitive luminescence components, particularly for quartz components. The most photosensitive traps for quartz are reset within 10 seconds of high-intensity (25mW/cm^2) blue light (470 ± 20nm) exposure (*S17*). These same traps are linked to the 325°C thermal luminescence peak, suggesting that its parent traps are thermally stable over geologic timescales (lifetime >3 x 10^7 years at 20°C) (*S15, S18*), and are thus suitable targets for luminescence dating studies. This dating study used the blue light emitting diode injection current that was limited to 10% of maximum, minimizing the photo-stimulation intensity and spreading the contributions from the various photosensitive traps over a much longer time period (20 seconds), increasing component resolution. The resulting distributions of the natural luminescence response with increasing photo-stimulation time for the Debra L. Friedkin Site sediments suggested full solar resetting, with a preheat treatment of 150°C for 1 hour yielding a luminescence distribution most similar to the natural emissions (Fig. S4).

The MAR procedure (Table S1) determined one equivalent dose for each sample initially after infrared (IR) stimulation, and then followed by blue stimulation (post IR-blue), similar to the so-called double, single aliquot regeneration protocols (*S19, S20*). The post-IR blue emissions may provide a more robust chronologic metric because initial infrared stimulation may

reduce the feldspar luminescence signal, which is implicated in anomalous fading and age underestimates, whereas the subsequent blue excitation is believed to resolve the time-stable quartz luminescence (cf. *S19, S20*). Debra L. Friedkin samples showed a dominance of emissions with blue-light excitation which was 2 to 10 times the emissions from infrared excitation. However, the efficacy of post-infrared blue stimulation on isolating the quartz emissions has been questioned because of the dominance of the feldspar signal, which may show instability and lead to age underestimates (*S10*). To evaluate the consistency of ages by post-IR blue stimulation, the corresponding quartz separate for seven samples was analyzed under blue excitation. It is important to note that ages by these two separate analytical approaches, post IR-blue and blue excitation of quartz separates, overlap at one standard deviation, providing a consistent chronology (Table S2).

Single aliquot regeneration protocols

Single aliquot regeneration (SAR) protocols (*S2*) were used in optical dating of fine-grained quartz separates (1 cm plate area) (Table S3). An Automated Risø TL/luminescence-DA-15 system was used for SAR analyses. Blue light excitation (470 ± 20 nm) was from an array of 30 light-emitting diodes that delivers ~15 mW/cm2 to the sample position at 90% power. A Thorn EMI 9235 QA photomultiplier tube coupled with three 3 mm thick Hoya U-340 detection filters, transmitting between 290 and 370 nm, measured photon emissions. Laboratory irradiations used a calibrated 90Sr/90Y beta source coupled with the Risø reader. The luminescence emissions for all quartz aliquots showed a clear dominance of a fast component (cf. *S2*) with > 95% diminution of luminescence after four seconds of excitation with blue light (Fig. S6a). All SAR emissions were integrated over the first 0.8 s of stimulation out of 40 s of measurement, with background based on emissions for the last 30- to 40-s interval.

A series of experiments was performed to evaluate the effect of preheating at 180°, 200°, 220° and 240°C on thermal transfer of the regenerative signal prior to the application of SAR dating protocols (cf. *S2*). These experiments showed no preheat-based sensitivity changes and a preheat temperature of 220°C was used in SAR analyses. A test for dose reproducibility was also performed (cf. *S2*) with the initial and final regenerative dose of 6.7 Gy yielding concordant luminescence response (at 1-sigma error) (Fig. S6). Calculation of equivalent dose by the single aliquot protocols was straightforward with at least 30 aliquots measured for each equivalent dose determination (Table S2). Equivalent dose distributions are unimodal (Fig. S6) and the common age model (*S21*) was utilized for final equivalent dose calculation.

Dose rate

To render an optical age, the environmental dose rate is needed, which is an estimate of sediment exposure to ionizing radiation from the decay of the U and Th series and ^{40}K, and cosmic sources during the burial period (Table S2). The U and Th content of sediment assuming secular equilibrium in the decay series and ^{40}K were determined by inductively coupled plasma-mass spectrometry analysed by Activation Laboratory LTD, Ontario, Canada. A small cosmic ray component of 0.20 to 0.16 mGy/yr for the indicated depth was included in the estimated dose rate (*S22*). Moisture content (by weight) for the dated sediment reflects current values at the Friedken site and a four year average at a nearby locality with similar soils. Moisture values vary from 40 to 35% with depth and are used appropriately in the final age calculations.

The dose rate for each sample level in a stratigraphic unit is highly consistent and overlaps at one standard deviation (see Table S2). Uranium values are in turn are very similar down profile with no depth trends, indicating little to none translocation. Uranium and thorium ratios are also consistent between 4 and 5 and coherent with an ultimate crustal source (*S23*). There is no evidence in the geochemical analyses (major, minor and rare earth elements) for dose rate inconsistencies associated with these sediments. We contend the radioactive disequilibrium, if present, is a secondary effect and well within the one sigma error of the associated age.

References

S1. M. Jain, L. Bøtter-Jensen, A. K. Singhvi, *Rad. Meas*. **37,** 67 (2003).

S2. A. S. Murray, A. G. Wintle, *Rad. Meas*, **37,** 377 (2003).

S3. H. M. Luchsinger, *Micromorphological Analysis of the Sediments and Soils from the Gault Site, a Clovis Site in Central Texas* (Thesis, Texas A&M University, College Station, 2002).

S4. P. Goldberg, in *Wilson-Leonard: An 11,000-year Archaeological Record of Hunter-Gatherers in Central Texas, Vol. 3: Artifacts and Special Artifact Studies*, M. B. Collins, Ed. (Studies in Archaeology 31. Texas Archaeological Research Laboratory, University of Texas, Austin, 1998), pp. 1343-1369.

S5. M. C. Rabenhorst, L. P. Wilding, L. T. West, *Soil Sci. Soc. Am. J.* **48,** 125-132 (1984).

S6. L. T. West, *Genesis of Soils and Carbonate Enriched Horizons Associated with Soft Limestones in Central Texas* (Dissertation, Texas A&M University, College Station, 1986).

S7. D. K. Koul, *Pramana-J. Phys*. **71,** 1209-1229 (2008).

S8. M. J. Aitken, *An Introduction to Optical Dating: The dating of Quaternary Sediments by the use of Photon-stimulated luminescence* (Oxford University Press, New York, 1998).

S9. G. W. Berger, P. J. Mulhern, D. H. Huntley, *Ancient TL* **18**, 7 (1980).

S10. H. M. Roberts, *Rad. Meas*. **42**, 1627 (2007).

S11. C. A. Richardson, *Rad. Meas*, **23**, 587 (1994).

S12. R. M. Bailey, J. S. Singarayer, S. Ward, S. Stokes, *Rad. Meas.* **37**, 511 (2003).

S13. S. L. Forman, J. Pierson, *Palaeogeog. Palaeoclimat. Palaeoecol*. **186**, 25. (2002).

S14. J.R. Wood, S. L. Forman, J. Pierson, J. Gomez, *Quat. Res*. **73**, 374 (2010).

S15. A. G. Wintle, A. S. Murray, *Rad. Meas.* **32**, 387 (2000).

S16. J. S. Singarayer, R. M. Bailey, *Rad. Meas*. **37(4-5)** 451-458 (2003).
S17. N. Agersnap-Larsen, E. Bulur, S. W. S. McKeever, *Rad. Meas* **32(5-6)**, 419-425 (2000).

S18. E. Bulur, L. Bøtter-Jensen, A. S. Murray, *Rad. Meas.* **32 (5-6)**, 407 (2000).

S19. D. Banerjee, A.S. Murray, L. Bøtter-Jensen, A. Lang, *Rad. Meas.* **33(1)**, 73 (2001).

S20. H. M. Roberts, A. G. Wintle, B. A. Maher, M.Y. Hu, *Holocene* **11,** 477 (2001).

S21. R. F. Galbraith, R.G. Roberts, G. M. Laslett, H. Yoshida, J. M. Olley, *Archaeometry* **41**, 339 (1999).

S22. J. R. Prescott, J. T. Hutton, *Rad. Meas.* **23**, 497 (1994).

S23. T. J. Ahrens, *Global Earth Physics, A Handbook of Physical Constants, AGU Reference Shelf 1* (American Geophysical Union, Washington, D.C., 1995).

S24. M. J. Aitken, S.G. E. Bowman, *Archaeometry* **17,** 132 (1975).

Table S1. Multiple Aliquot Regenerative Dose Procedure.

Growth Curve	Natural
1. Optical bleaching 8 hr sunlamp	1. Stimulation with infrared
2. Test dose 4 grays	2. Stimulation with blue light and data collection
3. Preheat 150° C for 1 hr	3. Optical bleaching 8 hr sunlamp
4. Stimulation with infrared	4. Test dose 4 Gy
5. Stimulation with blue light and data collection	5. Preheat 150° C for 1 hr
6. Optical bleaching 8 hr sunlamp	6. Stimulation with infrared
7. Regenerative doses (up to 165 grays)	7. Stimulation with blue light and data collection
8. Preheat 150° C for 1 h	
9. Stimulation with infrared	
10. Stimulation with blue light and data collection	

Table S2. Optically Stimulated Luminescence Ages on Fluvial Sediments from the Debra L. Friedkin Site, Texas.

Field Number	Laboratory Number	D_e (Gy) [a]	U (ppm) [b]	Th (ppm) [b]	K_20 (%) [b]	a value [c]	H_20 (%)	cosmic (mGy/yr) [d]	Dose Rate (mGy/yr)	Optical age (yr)
BC06-01	UIC1850	63.69 ± 3.10	2.5 ± 0.1	11.4 ± 0.1	0.73 ± 0.02	0.070 ± 0.007	40 ± 5	0.18 ± 0.02	2.24 ± 0.10	28,110 ± 2190
BC06-02	UIC1940	10.03 ± 0.62	2.8 ± 0.1	12.4 ± 0.1	1.28 ± 0.02	0.035 ± 0.004	35 ± 5	0.18 ± 0.02	2.59 ± 0.13	3870 ± 250
BC06-03	UIC1938	5.04 ± 0.35	1.4 ± 0.1	5.4 ± 0.1	0.58 ± 0.02	0.039 ± 0.004	35 ± 5	0.18 ± 0.02	1.28 ± 0.06	3940 ± 270
BC06-04	UIC1851	47.90 ± 2.50	2.8 ± 0.1	12.7 ± 0.1	0.74 ± 0.02	0.040 ± 0.004	40 ± 5	0.18 ± 0.02	2.25 ± 0.10	21,320 ± 1370
BC06-05	UIC1936	8.57 ± 0.55	2.3 ± 0.1	9.2 ± 0.1	0.91 ± 0.02	0.039 ± 0.004	35 ± 5	0.19 ± 0.02	2.01 ± 0.10	4255 ± 280
BC06-06	UIC1852	18.82 ± 1.01	2.0 ± 0.1	9.3 ± 0.1	0.69 ± 0.02	0.040 ± 0.004	40 ± 5	0.18 ± 0.02	1.76 ± 0.08	10,680 ± 700
BC06-07	UIC1853	21.00 ± 1.12	2.4 ± 0.1	9.6 ± 0.1	0.82 ± 0.02	0.040 ± 0.004	40 ± 5	0.18 ± 0.02	1.92 ± 0.09	10.940 ± 710
BC07-01	UIC2057	55.17 ± 2.17	2.7 ± 0.1	11.8 ± 0.1	1.17 ± 0.02	0.038 ± 0.003	40 ± 5	0.18 ± 0.02	2.27 ± 0.10	24,420 ± 1580
BC07-02	UIC2058	39.25 ± 1.89	2.4 ± 0.1	10.5 ± 0.1	0.91 ± 0.02	0.040 ± 0.003	40 ± 5	0.18 ± 0.02	1.93 ± 0.09	20,330 ± 1320
BC07-03	UIC2059	31.62 ± 1.46	2.4 ± 0.1	12.9 ± 0.1	1.18 ± 0.02	0.037 ± 0.004	38 ± 5	0.18 ± 0.02	2.42 ± 0.11	13,090 ± 830
BC07-03	UIC2059Q	33.10 ± 1.56	2.4 ± 0.1	12.9 ± 0.1	1.18 ± 0.02	0.035 ± 0.004	38 ± 5	0.18 ± 0.02	2.40 ± 0.11	13,780 ± 885
BC07-04	UIC2060	22.18 ± 1.03	2.7 ± 0.1	13.9 ± 0.1	1.31 ± 0.02	0.042 ± 0.003	36 ± 5	0.19 ± 0.02	2.75 ± 0.13	8070 ± 520
BC07-04	UIC2060Q	23.19 ± 1.13	2.7 ± 0.1	13.9 ± 0.1	1.31 ± 0.02	0.040 ± 0.003	36 ± 5	0.19 ± 0.02	2.72 ± 0.13	8490 ± 560
BC07-05	UIC2061	24.52 ± 1.13	2.5 ± 0.1	12.5 ± 0.1	1.18 ± 0.02	0.060 ± 0.004	36 ± 5	0.19 ± 0.02	2.66 ± 0.13	9215 ± 620
BC07-06	UIC2052	24.65 ± 1.13	2.9 ± 0.1	13.8 ± 0.1	1.23 ± 0.02	0.035 ± 0.004	36 ± 5	0.19 ± 0.02	2.67 ± 0.13	9250 ± 600
BC07-07	UIC2051	28.68 ± 1.36	2.7 ± 0.1	14.8 ± 0.1	1.31 ± 0.02	0.037 ± 0.003	37 ± 5	0.18 ± 0.02	2.74 ± 0.13	10,480 ± 675
BC07-08	UIC2050	31.53 ± 1.44	2.7 ± 0.1	11.5 ± 0.1	1.16 ± 0.02	0.040 ± 0.004	37 ± 5	0.18 ± 0.02	2.44 ± 0.11	12,910 ± 830
BC07-09	UIC2048	30.48 ± 1.40	2.5 ± 0.1	12.7 ± 0.1	1.20 ± 0.02	0.030 ± 0.003	37 ± 5	0.18 ± 0.02	2.40 ± 0.11	12,690 ± 955
BC07-11	UIC2045	29.58 ± 1.39	2.6 ± 0.1	13.4 ± 0.1	1.22 ± 0.02	0.025 ± 0.003	38 ± 5	0.18 ± 0.02	2.42 ± 0.11	12,240 ± 800
BC07-11	UIC2045Q	31.82 ± 1.56	2.6 ± 0.1	13.4 ± 0.1	1.22 ± 0.02	0.030 ± 0.003	38 ± 5	0.18 ± 0.02	2.46 ± 0.11	12,925 ± 845
BC07-12[f]	UIC2046	34.47 ± 1.58	2.6 ± 0.1	13.4 ± 0.1	1.13 ± 0.02	0.030 ± 0.003	38 ± 5	0.18 ± 0.02	2.40 ± 0.10	14,350 ± 910
BC07-13[f]	UIC2047	33.61 ± 1.53	2.5 ± 0.1	11.7 ± 0.1	1.06 ± 0.02	0.030 ± 0.003	38 ± 5	0.18 ± 0.02	2.20 ± 0.10	15,270 ± 960
BC07-14[f]	UIC2043	39.99 ± 1.85	2.7 ± 0.1	14.6 ± 0.1	1.29 ± 0.02	0.030 ± 0.003	39 ± 5	0.18 ± 0.02	2.63 ± 0.13	15,210 ± 960
BC07-15[f]	UIC2044	39.26 ± 1.81	2.5 ± 0.1	13.2 ± 0.1	1.14 ± 0.02	0.035 ± 0.003	39 ± 5	0.17 ± 0.02	2.39 ± 0.10	16,400 ± 1040
BC07-15[f]	UIC2044Q	37.12 ± 1.96	2.5 ± 0.1	13.2 ± 0.1	1.14 ± 0.02	0.030 ± 0.003	39 ± 5	0.17 ± 0.02	2.35 ± 0.10	15,800 ± 1080
BC07-16[f]	UIC2062	40.42 ± 1.89	2.6 ± 0.1	13.4 ± 0.1	1.22 ± 0.02	0.040 ± 0.004	40 ± 5	0.16 ± 0.02	2.50 ± 0.12	16,170 ± 1030
BC07-18[e,f]	UIC2183	35.56 ± 1.65	2.6 ± 0.1	12.7 ± 0.1	1.08 ± 0.02	0.040 ± 0.004	40 ± 5	0.16 ± 0.02	2.35 ± 0.11	15,110 ± 960
BMC08-01	UIC2378	16.40 ± 0.74	2.3 ± 0.1	8.1 ± 0.1	0.69 ± 0.02	0.032 ± 0.003	40 ± 5	0.20 ± 0.02	1.66 ± 0.08	9860 ± 740
BMC08-02	UIC2379	31.52 ± 1.55	2.4 ± 0.1	9.9 ± 0.1	0.59 ± 0.02	0.025 ± 0.002	40 ± 5	0.19 ± 0.02	1.68 ± 0.08	18,770 ± 1460
BMC08-03	UIC2380	51.91 ± 2.46	2.2 ± 0.1	8.8 ± 0.1	0.52 ± 0.02	0.040 ± 0.004	40 ± 5	0.17 ± 0.02	1.61 ± 0.08	32,290 ± 2520
BMC08-04	UIC2381	70.76 ± 3.31	2.6 ± 0.1	9.8 ± 0.1	0.69 ± 0.02	0.030 ± 0.003	40 ± 5	0.17 ± 0.02	1.81 ± 0.09	39,140 ± 2510
BMC08-05	UIC2382	22.42 ± 1.08	2.4 ± 0.1	9.1 ± 0.1	0.82 ± 0.02	0.054 ± 0.005	40 ± 5	0.17 ± 0.02	1.97 ± 0.09	11,360 ± 840
BMC08-06	UIC2383	27.27 ± 1.29	2.5 ± 0.1	10.6 ± 0.1	0.80 ± 0.02	0.037 ± 0.005	40 ± 5	0.17 ± 0.02	1.97 ± 0.09	13,855 ± 1015
BMC08-07	UIC2360	19.59 ± 0.93	2.7 ± 0.1	12.8 ± 0.1	1.43 ± 0.02	0.040 ± 0.004	36 ± 5	0.19 ± 0.02	2.73 ± 0.12	7160 ± 470
BMC08-07	UIC2360S	19.23 ± 0.94	2.7 ± 0.1	12.8 ± 0.1	1.43 ± 0.02	0.040 ± 0.004	36 ± 5	0.19 ± 0.02	2.73 ± 0.12	7030 ± 470
BMC08-08	UIC2362	21.11 ± 1.01	2.5 ± 0.1	11.6 ± 0.1	1.26 ± 0.02	0.053 ± 0.004	36 ± 5	0.19 ± 0.02	2.59 ± 0.12	8160 ± 540
BMC08-09	UIC2361	20.22 ± 1.07	2.7 ± 0.1	12.5 ± 0.1	1.39 ± 0.02	0.040 ± 0.003	37 ± 5	0.19 ± 0.02	2.66 ± 0.12	7600 ± 500
BMC08-10	UIC2 363	24.85 ± 1.18	2.8 ± 0.1	13.0 ± 0.1	1.28 ± 0.02	0.040 ± 0.003	37 ± 5	0.19 ± 0.02	2.64 ± 0.12	9405 ± 610
BMC08-11	UIC2364	25.96 ± 1.22	2.8 ± 0.1	13.0 ± 0.1	1.27 ± 0.02	0.040 ± 0.003	37 ± 5	0.19 ± 0.02	2.61 ± 0.12	9930 ± 640
BMC08-12	UIC2365	30.74 ± 1.43	2.8 ± 0.1	12.9 ± 0.1	1.31 ± 0.02	0.035 ± 0.003	38 ± 5	0.19 ± 0.02	2.59 ± 0.12	11,870 ± 760

Field Number	Laboratory Number [a]	D_e (Gy)	U (ppm) [b]	Th (ppm) [b]	K_20 (%) [b]	a value [c]	H_20 (%)	cosmic (mGy/yr) [d]	Dose Rate (mGy/yr)	Optical age (yr)
BMC08-13	UIC2366	32.58 ± 1.54	3.0 ± 0.1	13.2 ± 0.1	1.28 ± 0.02	0.044 ± 0.003	38 ± 5	0.18 ± 0.02	2.72 ± 0.12	12,000 ± 770
BMC08-13	UIC2366S	32.36 ± 1.80	3.0 ± 0.1	13.2 ± 0.1	1.28 ± 0.02	0.040 ± 0.004	38 ± 5	0.18 ± 0.02	2.67 ± 0.12	12,100 ± 860
BMC08-14[f]	UIC2354	35.89 ± 1.71	2.9 ± 0.1	12.2 ± 0.1	1.15 ± 0.02	0.050 ± 0.004	39 ± 5	0.18 ± 0.02	2.55 ± 0.12	14,070 ± 910
BMC08-15[f]	UIC2367	35.67 ± 1.72	2.7 ± 0.1	11.9 ± 0.1	1.16 ± 0.02	0.055 ± 0.004	39 ± 5	0.18 ± 0.02	2.53 ± 0.12	14,080 ± 920
BMC08-16[f]	UIC2369	35.94 ± 1.73	4.1 ± 0.1	10.6 ± 0.1	0.96 ± 0.02	0.040 ± 0.003	39 ± 5	0.18 ± 0.02	2.50 ± 0.12	14,370 ± 930
BMC08-17[f]	UIC2350	29.98 ± 1.40	2.6 ± 0.1	10.5 ± 0.1	1.00 ± 0.02	0.036 ± 0.004	39 ± 5	0.18 ± 0.02	2.14 ± 0.10	14,000 ± 890
BMC08-17[f]	UIC2350Q	30.88 ± 1.39	2.6 ± 0.1	10.5 ± 0.1	1.00 ± 0.02	0.035 ± 0.003	39 ± 5	0.18 ± 0.02	2.13 ± 0.10	14,480 ± 920
BMC08-17[f]	UIC2350S	31.10 ± 1.72	2.6 ± 0.1	10.5 ± 0.1	1.00 ± 0.02	0.035 ± 0.003	39 ± 5	0.18 ± 0.02	2.13 ± 0.10	14,580 ± 1030
BMC08-18[f]	UIC2359	38.39 ± 1.82	2.8 ± 0.1	11.6 ± 0.1	1.16 ± 0.02	0.044 ± 0.003	39 ± 5	0.18 ± 0.02	2.44 ± 0.11	15,730 ± 1010
BMC08-19[f]	UIC2356	37.73 ± 1.81	2.9 ± 0.1	12.6 ± 0.1	1.25 ± 0.02	0.040 ± 0.004	39 ± 5	0.18 ± 0.02	2.57 ± 0.11	14,710 ± 940
BMC08-20[f]	UIC2368	40.82 ± 1.95	2.8 ± 0.1	10.8± 0.1	1.01 ± 0.02	0.050 ± 0.005	39 ± 5	0.18 ± 0.02	2.33 ± 0.10	17,530 ± 1140
BMC08-21[f]	UIC2553	38.98 ± 1.83	3.0 ± 0.1	11.6 ± 0.1	1.08 ± 0.02	0.040 ± 0.004	39 ± 5	0.18 ± 0.02	2.40 ± 0.10	16,270 ± 1040
BMC08-22[f]	UIC2355	38.20 ± 1.85	2.6 ± 0.1	11.2 ± 0.1	1.02 ± 0.02	0.05o ± 0.005	39 ± 5	0.18 ± 0.02	2.31 ± 0.10	16,515 ± 1075
BMC08-23	UIC2348	45.68 ± 2.16	3.0 ± 0.1	12.2 ± 0.1	1.12 ± 0.02	0.036 ± 0.004	40 ± 5	0.18 ± 0.02	2.41 ± 0.10	18,930 ± 1210
BMC08-24	UIC2370	46.07 ± 2.20	3.0 ± 0.1	11.8 ± 0.1	0.90 ± 0.02	0.037 ± 0.004	40 ± 5	0.18 ± 0.02	2.24 ± 0.10	20,565 ± 1325
BMC08-24	UIC2370Q	45.90 ± 2.15	3.0 ± 0.1	11.8 ± 0.1	0.90 ± 0.02	0.037 ± 0.004	40 ± 5	0.18 ± 0.02	2.24 ± 0.10	20,490 ± 1305
BMC08-25	UIC2357	48.23 ± 2.26	2.5 ± 0.1	10.0 ± 0.1	1.04 ± 0.02	0.040 ± 0.004	40 ± 5	0.18 ± 0.02	2.12 ± 0.10	22,710 ± 1450
BMC08-25	UIC2357S	51.48 ± 2.77	2.5 ± 0.1	10.0 ± 0.1	1.04 ± 0.02	0.035 ± 0.003	40 ± 5	0.18 ± 0.02	2.22 ± 0.10	23,150 ± 1600
BMC08-26	UIC2358	53.84 ± 0.40	3.0 ± 0.1	9.8 ± 0.1	0.86 ± 0.02	0.045 ± 0.004	40 ± 5	0.18 ± 0.02	2.14 ± 0.10	25,185 ± 1640
BMC08-27	UIC2351	64.10 ± 3.03	3.4 ± 0.1	11.6 ± 0.1	1.01 ± 0.02	0.044 ± 0.004	40 ± 5	0.18 ± 0.02	2.46 ± 0.11	26,090 ± 1670
BMC08-27	UIC2351Q	68.17 ± 3.26	3.4 ± 0.1	11.6 ± 0.1	1.01 ± 0.02	0.045 ± 0.004	40 ± 5	0.18 ± 0.02	2.46 ± 0.11	27,650 ± 1800
BMC08-28	UIC2349	73.16 ± 3.51	3.7 ± 0.1	10.1 ± 0.1	0.85 ± 0.02	0.036 ± 0.004	40 ± 5	0.18 ± 0.02	2.24 ± 0.10	32,720 ± 2110
BMC08-29	UIC2352	2.60 ± 0.13	3.0 ± 0.1	9.2 ± 0.1	1.15 ± 0.02	0.053 ± 0.005	30 ± 5	0.20 ± 0.02	2.60 ± 0.13	1000 ± 70

[a] Equivalent dose (D_e) determined by the multiple aliquot regenerative dose technique (Jain et al. 2003) with initial infrared (880 ± 40 nm) excitation, followed by blue light (470 ± 20 nm) excitation on the polymineral fine-grained fraction (4-11 micron). Q designation indicates equivalent dose determined on the fine-grained (4-11 micron) quartz fraction by the multiple aliquot regenerative dose technique under blue light excitation. S indicates analysis of the fine-grained (4-11 micron) quartz fraction by single aliquot regeneration protocols (*S2*), with 30 aliquots measured with blue light excitation.

[b] U, Th and K_20 assayed by ICP-MS at Activation Laboratories, Ontario, Canada.

[c] Measured alpha efficiency factor (a value) (*S24*).

[d] Ages included a cosmic ray dose rate (*S22*). All errors are at one sigma.

[e] Age associated with a biface from Level 35a.

[f] Ages associated with the Buttermilk Creek Complex.

Table S3. Single Aliquot Regeneration Protocols for Optical Dating.

Step	Treatment
1	Natural dose or give beta dose
2	Preheat (e.g. 220º C for 10s)
3	Stimulate with blue light (470 nm) for 40s at 125º C
4	Give beta test dose (e.g. 0.5 Gray)
5	Preheat as in step 2
6	Stimulate with blue light (470 nm) for 40s at 125º C
7	Stimulate with blue light for 40s at 260º C
8	Return to step 1

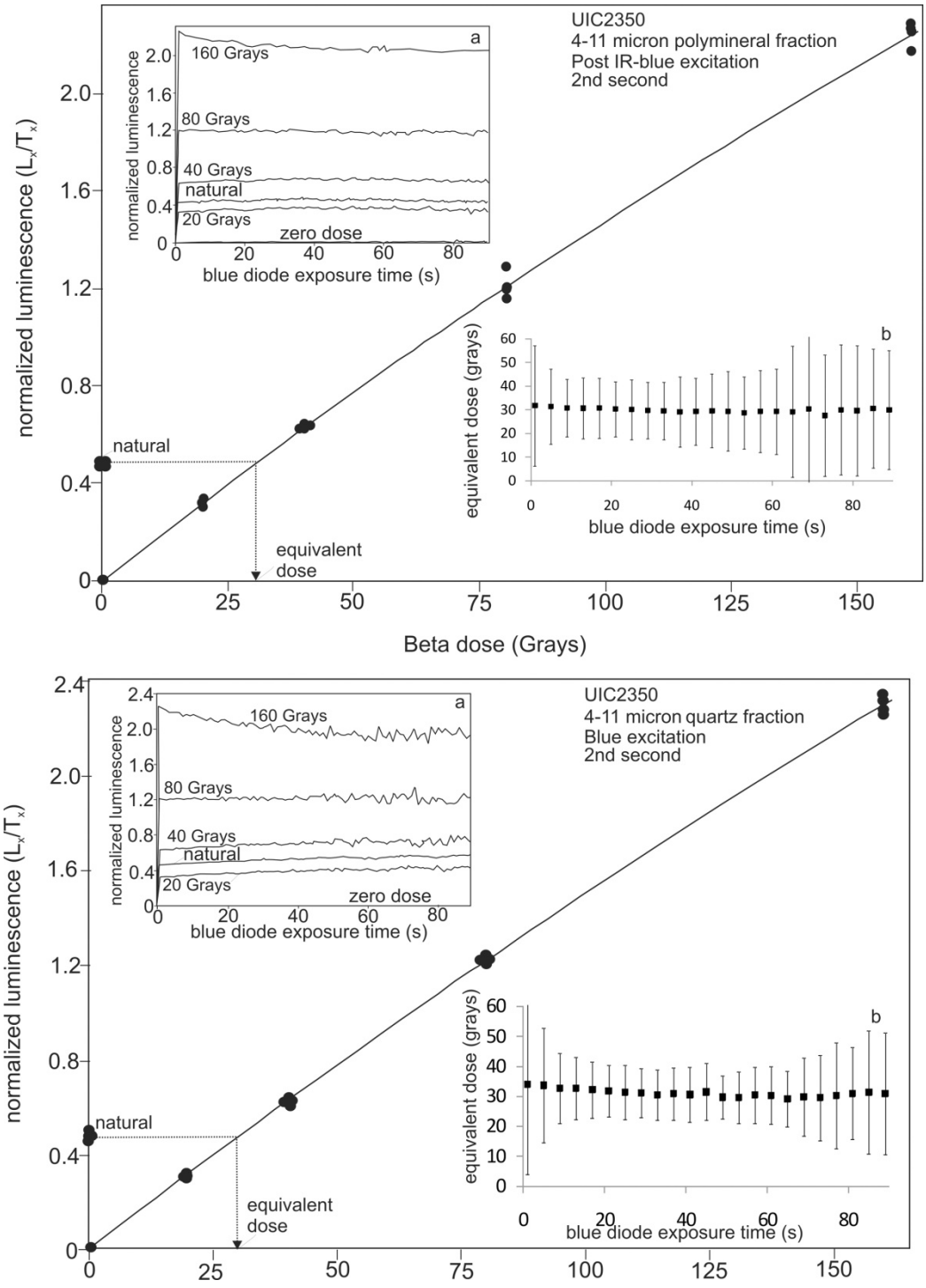

Figure S4. Regenerative dose response curve for sample UIC2350 from a finely-laminated silt. Upper figure is for the fine-grained (4-11 micron) polymineral extract, lower for corresponding quartz extract. Inset figures (a) show natural luminescence normalized shine down curves and associated regenerative dose response. Inset figures (b) shows equivalent dose for multiple light exposure times (plateau plot), including after 2 s, which is depicted in the main plot.

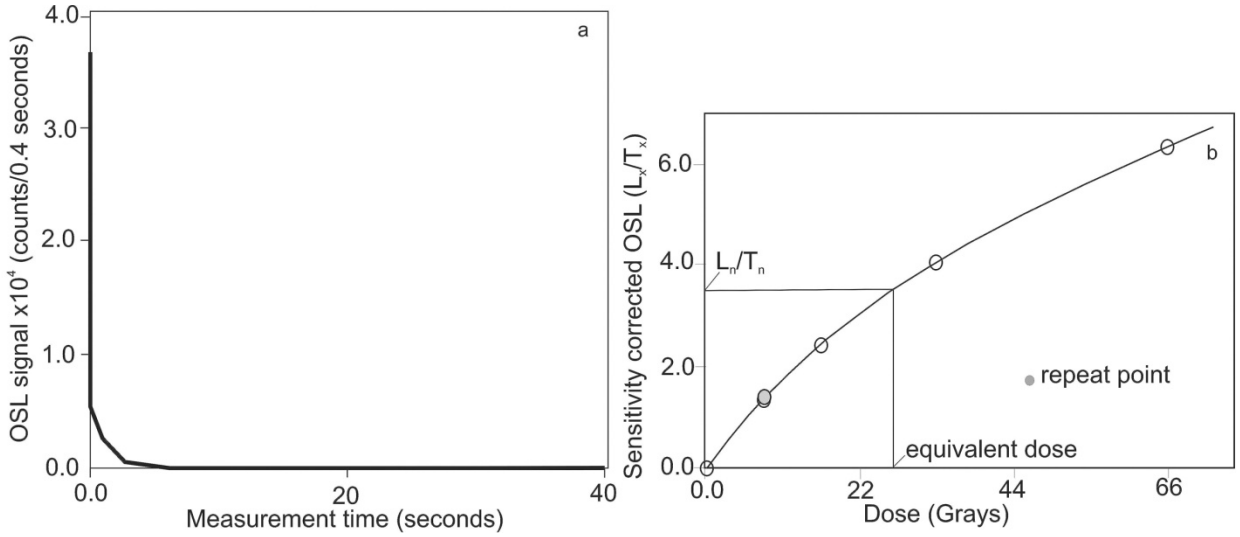

Figure S5. Luminescence data for the 4-11 micron quartz aliquots for sample UIC2350 (a) Optical decay curve measured using blue emitting diodes (470 +/- 20 nm) for natural luminescence. (b) Dose response curve.

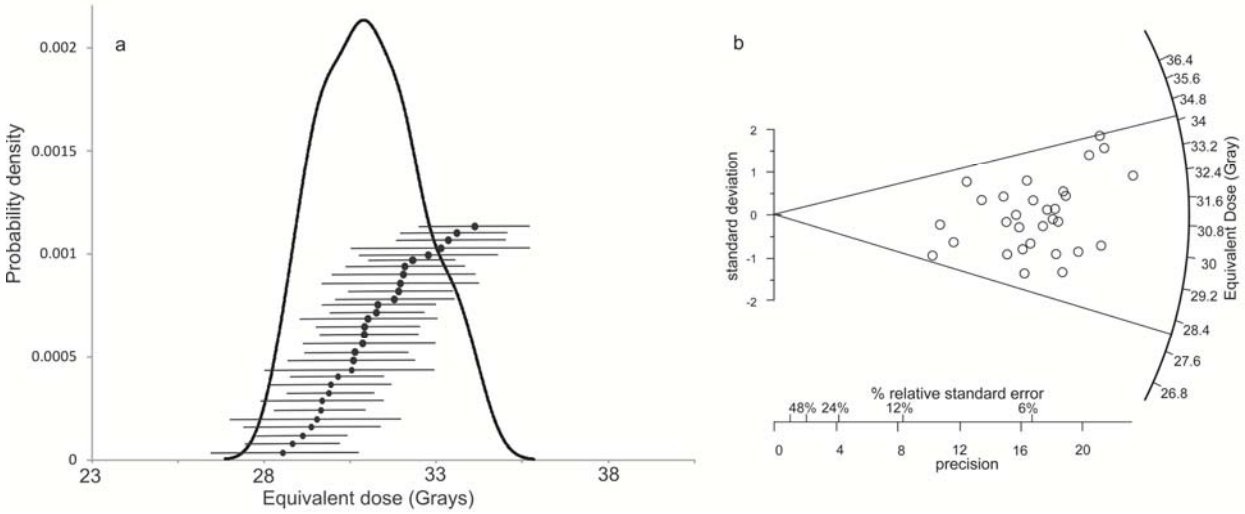

Figure S6. (a) Probability density distribution of 30 equivalent dose determinations for sample UIC2350. (b) Radial plot of equivalent dose data as in (a); lines forming the wedge indicates 2 sigma limit.

Pedologic Analysis

Morphological Features

The floodplain soil has an A-Bss-2Bk horizon sequence in both the microlow and microhigh (Tables S4 & S5). Field morphological descriptions following standards of the Soil Survey Division Staff (*S25*) reveal systematic depth functions without inflections or inversion related to shrink-swell processes. Color gradually changes from black to brown in response to decreasing organic matter content. Ped structure shifts from medium subangular blocky in surface horizons to coarse wedge and angular blocky in subsurface horizons. A few iron-manganese concretions and soft iron masses near the contact between the alluvial parent material and underlying colluvium suggest brief periods of iron reduction (*S26*), but have no bearing on site formation. Weakly expressed, low angle (< 25°) slickensides accompanied by minimal grooving of ped surfaces points to limited swelling pressures from wetting. Coarse fragments are comprised principally of lithic artifacts (chert) and limestone fragments. The calcic horizon begins in the colluvium (2Bk). The pedogenic $CaCO_3$ is derived from the overlying Bss horizons. The depth of pedogenic carbonate nodules is consistent with MAP of the study area of ~ 900 mm (*S27*).

Characterization Data

Bulk soil samples were collected from each described horizon and analyzed at the Texas A&M University Soil Characterization Laboratory for routine physical and chemical properties (*S28, S29*). Characterization data from both the microlow and microhigh confirms field morphological observations (Tables S6 & S7). Clay content is relatively uniform with depth until the colluvial layer is encountered, and coarse fragments generally track lithic artifacts and limestone fragments. The pH follows the depth distribution of detrital and pedogenic calcium carbonate content, which reflects a noncalcareous upper profile from leaching and a calcareous subsoil from accumulation. The low bulk densities are typical for clay-rich soils with high microporosity (*S30*), where COLE values are high because of the shrink-swell potential as evidenced by appreciable differences in bulk density between moist and dry states. Importantly, organic carbon content decreases systematically with depth without inflection until the colluvial layer.

Differences in properties between the microlow and microhigh indicate differential water flux as regulated by subsurface microtopography. This is noticeable in the microlow where pH and $CaCO_3$ content reflect a slightly greater depth of leaching because of preferential funneling of water into this part of the pedon.

Micromorphological Features

Micromorphological analysis was conducted at the Baylor University Department of Geology on commercially prepared 5 x 7 cm oriented thin sections from each soil horizon described in the field, using an Olympus BX-51 research microscope equipped with a 12.5 MPx digital camera. Terminology for description follows Brewer (*S31*). Micromorphological observations were consistent with field observations of size and abundance of cracks and micro-artifacts. Crack aperture and abundance diminishes with depth and at the Clovis level is smaller

(< 1 mm diameter) than the majority of microartifacts, indicating that the microartifacts were unlikely to have reworked within cracks from higher to lower levels. Occurrences of micro-artifacts in the Buttermilk Creek Complex and Clovis levels thus indicate human activity during these time intervals. Shrink-swell related micro-fabrics (sepic-plasmic fabrics of Brewer, *S31*), though present, are rather weakly developed in the Buttermilk Creek Complex and Clovis levels, consistent with field morphological descriptions. Micromorphological features do not differ significantly between microlow and microhigh soil profiles sampled. Chert micro-artifacts (microdebitage) are common, sand-sized (< 2 mm) and extend from the surface A horizon downward through all 5-6 Bss horizons. Grains are dominantly composed of finely crystalline chert and chalcedony, with more grains with Fe surface impregnations and weathering present in deeper horizons. There is no micromorphological evidence for downward translocation of macro-or micro-artifacts in the Buttermilk Creek Complex and Clovis levels within soil cracks.

Taxonomic Classification

Both the microlow and microhigh profiles classify as fine, smectitic, thermic Calcic Haplusterts according to soil taxonomic criteria (*S32*). The family particle size control section (25 to 100 cm depth) is fine because of more than 35% clay, smectitic because of high CEC values, CEC/clay ratios, and slickensides, and thermic because MAT at 50 cm depth is between 15 to 22°C. The Buttermilk Creek soil has a mollic epipedon (thick, dark, organic-enriched mineral layer), and cambic (ped structure and slickensides) and calcic (> 5% pedogenic carbonate nodules) subsurface diagnostic horizons. However, the calcic occurs at a depth greater than that recognized (>100 cm) at taxonomic levels above the subgroup. The Soil Survey of Bell County (*S33*) shows the Buttermilk Creek locality mapped as Lewisville silty clay, 1-3% slopes. The Lewisville is classified as a fine-silty, mixed, thermic Typic Calciustoll. Apparently, the higher clay content and slickensides identified in our study area were an inclusion within the soil map unit.

Clay content, slickensides, surface cracking, and evidence of subsurface microlow and microhigh topography indicate that the Block A floodplain soil is a Vertisol according to taxonomic criteria (*S32*). The old model of Vertisol formation assumes that churning, or self-swallowing, from sloughing of material into cracks during drying leads to volume expansion and the formation of randomly distributed slickensides to relieve swelling pressures during wetting (*S34*). This form of pedoturbation was thought to limit horizonation and systematic depth functions of key properties and led to the mixing of the soil matrix. This model of Vertisol formation is no longer valid and has been replaced by the mechanics model of Vertisol formation. In this case, the large volume of micropores in the clayey soil promotes expansion and contraction of the soil material through water intake and subsequent desiccation (*S35*). When swelling pressures exceed the particle shear strength, the mechanics model predicts that lateral translocation of soil material may occur from the subsoil of the microlow towards the upper part of the microhigh along master slickensides. In this case, random or vertical mixing is minimized. As a consequence, horizonation and systematic depth functions form, particularly in the microlow and are retained, with the principal weathering differences occurring between microlows and microhighs because of differential water flux (*S36*).

Interpretation

The systematic depth functions of clay, organic carbon, calcium carbonate, color, ped structure, and pH through the Debra L. Friedkin site Vertisol show that it is weakly developed and formed as a result of the mechanics model of Vertisol formation. Differences in properties between the microlow and microhigh, as regulated by water flux, are minimal and when coupled with the absence of surface gilgai features or master slickensides, demonstrate that little soil displacement has occurred. Crack infills (0.5-3 cm diameter) constitute a maximum of ~ 2 to 3% by volume of the microlow and ~ 10 to 12% by volume of the microhigh within the upper 100 cm. Crack diameter rapidly decreases to apertures of no more than 0.5 to 1 cm before disappearing at depths of > 100 cm. Significantly, soil material between the crack infills remains intact, independent of lateral or vertical shifting from shrink-swell processes, which is facilitated by the near absence of rodent burrows and limited root penetration (<2.0 mm diameter).

References

S25. Soil Survey Division Staff, *Soil Survey Manual, USDA Handbook 18* (U.S. Government Printing Office, 1993).

S26. M. J. Vepraskas, in *Wetland Soils: Genesis, Hydrology, Landscapes, and Classification*, M. J. Vepraskas, J. L. Richardson, Eds. (Lewis Publishers, Boca Raton, 2001), pp. 163–182.

S27. L. Nordt, M. Orosz, S. Driese, J. Tubbs, *J. Geol.***114**, 501 (2006).

S28. C. T. Hallmark, L. West, L. Wilding L. Drees, *Characterization Data for Selected Texas Soils, Miscellaneous Publication 1583* (Texas Agriculture Experiment Station, College Station,1986).

S29. http://soildata.tamu.edu/methods.pdf

S30. Soil Survey Staff, *Soil Survey Laboratory Information Manual, Soil Survey Investigations Report No. 45. Version 1.0. USDA-NRCS* (U.S. Government Printing Office, 1995).

S31. R. Brewer, *Fabric and Mineral Analysis of Soils* (Robert E. Krieger Publishing Company, New York, 1976).

S32. Soil Survey Staff, *Soil Taxonomy: A Basic System of Soil Classification for Making and Interpreting Soil Surveys, USDA-NRCS Handbook 436* (U.S. Government Printing Office, 1999).

S33. J. W. Huckabee, D. R. Thompson, J. C. Wyrick, E. G. Pavlat, *Soil Survey of Bell County, Texas: USDA-NRCS*, (U.S. Government Printing Office, 1977).

S34. S. Buol, F. Hole, R. McCracken, R. Southard, *Soil Genesis and Classification* (Iowa State University Press, Ames, 1997).

S35. L. Wilding, D. Tessier, in *Vertisols: Their Distribution, Properties, Classification and Management*, L. Wilding, R. Puentes, Eds. (Texas A&M University Printing Center, College Station, 1988), pp. 55–81.

S36. L. C. Nordt, S. G. Driese, *Hydrol. Earth Syst. Sci.* **13**, 2039 (2009).

Table S4. Field morphological description of pedon S07TX-027-001 (microlow). All color designations are for moist conditions unless otherwise stated.

A1 --- 0 to 15 cm; black (10YR 2/1) clay; moderate medium subangular blocky structure; very firm consistence; common fine roots; common (7%) chert fragments, angular to subangular, up to 2 cm diameter; noneffervescent; gradual smooth boundary.

A2 --- 15 to 32 cm; black (10YR 2/1) clay; moderate medium angular blocky structure; very firm consistence; common fine roots; pressure faces; common (5%) chert fragments, angular to subangular, up to 1.5 cm diameter; noneffervescent; gradual smooth boundary.

Bss1 --- 32 to 62 cm; very dark gray (10YR 3/1) clay; moderate coarse angular blocky and common medium wedge structure; firm; few fine roots; common (5%) distinct slickensides, 25° angle; common (6%) chert fragments, angular to subangular, up to 1 cm diameter; few (2%) black (10YR 2/1) crack infills, up to 2 cm diameter; noneffervescent; gradual smooth boundary.

Bss2 --- 62 to 75 cm; very dark grayish brown (10YR 3/2) clay; moderate coarse angular blocky and common medium wedge structure; firm consistence; very few fine roots; common (5%) distinct slickensides, 25° angle; common (6%) chert fragments, angular to subangular, up to 1 cm diameter; few (2%) black (10YR 2/1) crack infills, up to 2 cm diameter; noneffervescent; gradual smooth boundary.

Bss3 --- 75 to 86 cm; brown (10YR 4/3) clay; moderate coarse angular blocky and common medium wedge structure; firm consistence; very few fine roots; common (5%) distinct slickensides, 25° angle; common (6%) chert fragments, angular to subangular, up to 1 cm diameter; few (2%) black (10YR 2/1) crack infills, up to 2 cm diameter; noneffervescent; gradual smooth boundary.

Bss4 --- 86 to 100 cm; brown (10YR 4/3) clay; moderate coarse angular blocky and common medium wedge structure; firm consistence; very few fine roots; common (5%) distinct slickensides, 25° angle; few fine distinct strong brown (7.5YR 5/6) iron concentrations; common (4%) chert fragments, angular to subangular, up to 1 cm diameter; very few (1%) black (10YR 2/1) crack infills, up to 3 cm diameter; noneffervescent; few fine iron manganese concretions; gradual smooth boundary.

Bss5 --- 100 to 119 cm; brown (10YR 4/3) clay; moderate coarse angular blocky and common medium wedge structure; firm consistence; very few fine roots; few (2%) distinct slickensides, 25° angle; common (4%) chert fragments, angular to subangular, up to 3 cm diameter; slightly effervescent; few (1%) iron manganese concretions; clear smooth boundary.

2Bk1 --- 119 to 144 cm; reddish yellow (7.5YR 6/6) clay loam; weak coarse angular blocky; firm consistence; common (12%) limestone fragments, flaggy, 1 to 4 cm diameter; strongly effervescent; common (15%) soft masses of calcium carbonate, up to 1.5 cm diameter; abrupt smooth boundary.

2Bk2 --- 144 to 157 cm; reddish yellow (7.5YR 6/6) very gravelly clay loam; massive; firm consistence; many (40%) limestone fragments, flaggy, up to 6 cm diameter; strongly effervescent; common (4%) soft masses of calcium carbonate, up to 1.5 cm diameter.

Table S5. Field morphological properties of pedon S07TX-027-002 (microhigh). All color designations are for moist conditions unless otherwise stated.

A1 --- 0 to 17 cm; black (10RY 2/1) clay; moderate medium subangular blocky structure; very firm consistence; common fine and medium roots; common (6%) chert fragments, angular to subangular, up to 5 cm diameter; noneffervescent; gradual smooth boundary.

A2 --- 17 to 31 cm; very dark gray (10YR 3/1) clay; moderate medium angular blocky structure; very firm consistence; common fine and medium roots; common (6%) chert fragments, angular to subangular, up to 5 cm diameter; common (10%) black (10YR 2/1) crack infills, up to 2 cm diameter; noneffervescent; gradual smooth boundary.

Bss1 --- 31 to 47 cm; dark grayish brown (10YR 4/2) clay; moderate coarse angular blocky and few fine wedge structure; firm consistence; few fine roots; common (5%) distinct slickensides, 25° angle; common (6%) chert fragments, angular to subangular, up to 2 cm diameter; common (9%) black (10YR 2/1) crack infills, up to 2 cm diameter; noneffervescent; gradual smooth boundary.

Bss2 --- 47 to 63 cm; dark grayish brown (10 YR 4/2) clay; moderate coarse angular blocky and few medium wedge structure; firm consistence; few fine roots; common (5%) distinct slickensides, 25° angle; common (10%) chert fragments, angular to subangular, up to 2 cm diameter, some limestone; common (7%) black (10YR 2/1) crack infills, up to1 cm diameter; noneffervescent; gradual smooth boundary.

Bss3 --- 63 to 79 cm; dark grayish brown (10YR 4/2) clay; moderate coarse angular blocky and few medium wedge structure; firm consistence; few fine roots; common (5%) distinct slickensides, 25° angle; common (6%) chert fragments and few limestone fragments, angular to subangular, up to 1 cm diameter, common (6%) black (10YR 2/1) crack infills, up to 1 cm diameter; noneffervescent; gradual smooth boundary.

Bss4 --- 79 to 102 cm; brown (10YR 4/3) clay; moderate coarse angular blocky and few medium wedge structure; firm consistence; very few fine roots; common (5%) distinct slickensides, 25° angle; common (6%) chert fragments and few limestone fragments, angular to subangular, up to 1 cm diameter; common (5%) black (10YR 2/1) crack infills, up to 0.5 cm diameter; noneffervescent; gradual smooth boundary.

Bss5 --- 102 to 119 cm; brown (10YR 4/3) clay; weak coarse angular blocky structure; firm consistence; very few fine roots; common (5%) faint slickensides, 5° angle; common (5%) chert fragments and few limestone fragments, angular to subangular, up to 1 cm diameter; few fine black iron-manganese concretions; gradual smooth boundary.

Bss6 --- 119 to 130 cm; brown (10YR 4/3) clay; weak coarse angular blocky structure; firm consistence; very few fine roots; common (5%) faint slickensides, 5° angle; common (5%) medium distinct brownish yellow (10YR 6/6) iron concentrations; common (5%) chert and limestone fragments, angular to subangular, up to 1 cm diameter; slightly effervescent; few (2%) calcium carbonate nodules up to 1.5 cm diameter; few fine black concretions; clear smooth boundary.

2Bk --- 130 to 157 cm; brown (7.5YR 5/4) clay loam; weak coarse angular blocky structure; firm consistence; common (5%) medium distinct yellowish brown (10YR 5/6) iron concentration; common (10%) chert and limestone fragments up to 3 cm diameter; strongly effervescent; common (15%) calcium carbonate masses, up to1.5 cm diameter.

Table S6. Characterization data of pedon S07TX-027-001 (microlow).

			Particle Size Distribution (mm)									
			Sand	*Silt*	*Clay*	*Fragments*			Bulk Density			Organic
Lab	Depth	Horizon	(2.0-0.05)	(0.05-0.002)	(<0.002)	(>2.0)	pH	$CaCO_3$	*1/3 bar*	*Oven Dry*	COLE	Carbon
No.	(cm)		----------%----------				(H_2O)	(%)	---------g cm^{-3}--------		(cm cm^{-1})	(%)
7239	0-15	A1	6.0	45.9	48.1	12.0	6.8	0.0	1.05	1.59	0.148	4.01
7240	15-32	A2	4.9	34.9	60.2	2.0	7.1	0.0	1.11	1.77	0.168	1.96
7241	32-62	Bss1	6.6	35.4	58.0	5.0	7.5	0.0	1.11	1.73	0.159	1.40
7242	62-75	Bss2	6.7	36.1	57.2	5.0	7.5	0.0	1.11	1.70	0.153	1.61
7243	75-86	Bss3	9.6	34.8	55.6	11.0	7.8	5.5	1.13	1.68	0.141	0.75
7244	86-100	Bss4	10.9	33.5	55.6	8.0	7.8	5.9	1.13	1.65	0.134	0.55
7245	100-119	Bss5	10.7	33.6	55.7	9.0	7.8	8.6	1.10	1.67	0.149	0.49
7246	119-144	2Bk1	17.9	46.3	35.8	23.0	8.2	58.3	1.32	1.47	0.037	0.64
7247	144-157	2Bk2	19.8	51.9	28.3	56.0	8.3	67.3	1.16	1.23	0.020	0.38
7248	-	R	-	-	-	-	-	80.7	-	-	-	-

Table S7. Characterization data of pedon S07TX-027-002 (microhigh).

			Particle Size Distribution (mm)									
			Sand	*Silt*	*Clay*	*Fragments*			Bulk Density			Organic
Lab	Depth	Horizon	(2.0-0.05)	(0.05-0.002)	(<0.002)	(>2.0)	pH	$CaCO_3$	*1/3 bar*	*Oven Dry*	COLE	Carbon
No.	(cm)		----------%----------				(H_2O)	(%)	---------g cm^{-3}--------		(cm cm^{-1})	(%)
7249	0-17	A1	6.0	43.6	50.4	6.0	6.8	0.0	1.03	1.63	0.165	3.60
7250	17-31	A2	5.9	36.2	57.9	4.0	7.1	0.0	1.12	1.75	0.160	1.10
7251	31-47	Bss1	5.7	37.9	56.4	5.0	7.4	0.0	1.09	1.67	0.153	1.42
7252	47-63	Bss2	7.0	36.2	56.8	8.0	7.6	1.7	1.13	1.72	0.150	1.06
7253	63-79	Bss3	10.0	33.0	57.0	7.0	7.7	3.4	1.13	1.66	0.137	0.86
7254	79-102	Bss4	10.3	32.7	57.0	11.0	7.8	4.9	1.12	1.63	0.133	0.61
7255	102-119	Bss5	11.4	31.3	57.3	11.0	7.9	5.3	1.11	1.63	0.137	0.54
7256	119-130	Bss6	10.1	30.6	59.3	7.0	8.0	6.2	1.08	1.68	0.159	0.44
7257	130-157	2Bk	22.1	43.8	34.1	10.0	8.4	56.6	1.27	1.49	0.055	0.57

Magnetic Analyses

The evolution of magnetization within a floodplain soil begins with the initial deposition of magnetic particles during sedimentation and continues via subsequent alteration and growth of iron-bearing compounds by pedogenic and biologic means. Measurements of a soil's magnetic properties capture information about the complete developmental history of the soil, and are a convenient method by which to investigate pedogenesis. No rapid changes that could be associated with discrete depositional units or buried paleosols were observed. Magnetic analyses (Fig. S7) indicate no vertical mixing of sediments.

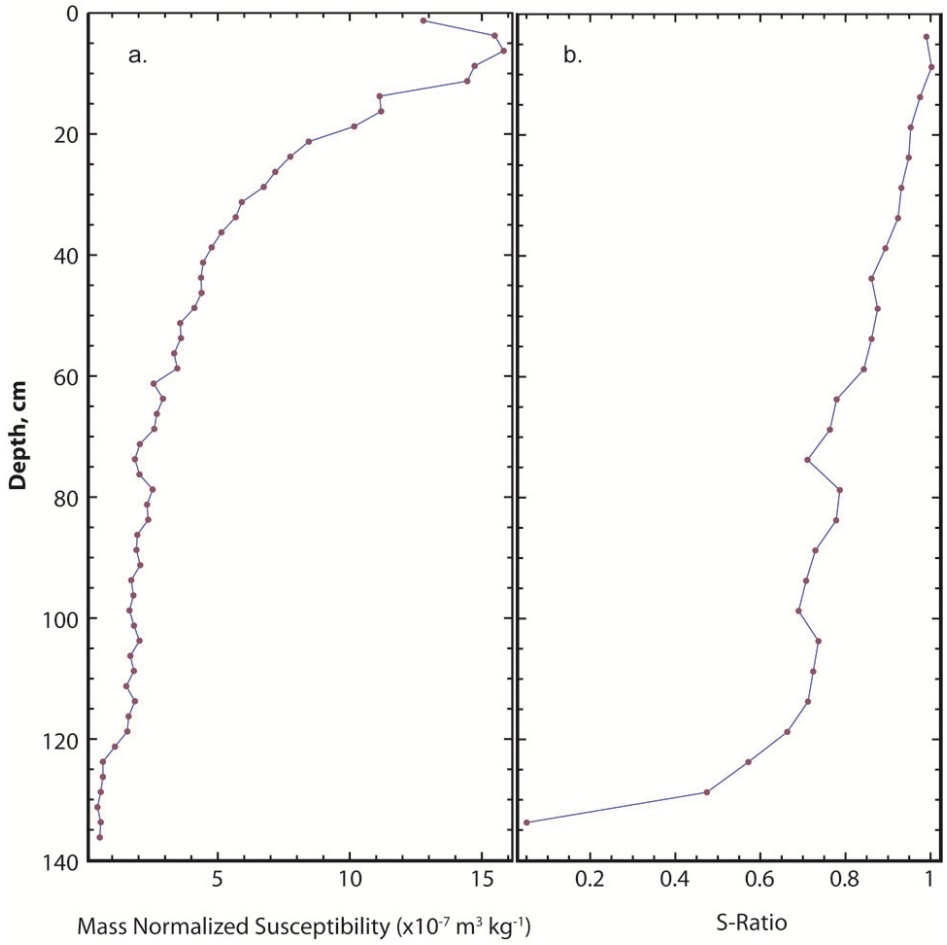

Figure S7. Magnetic properties of sediments within Block A (T-2). Samples were collected at the same location as luminescence column 1. (A) Magnetic susceptibility shows a gradual decrease with depth with no indications of buried soil horizons (paleosols) or soil disruption. (B) The S-ratio compares the magnetization held by magnetically 'soft' materials (e.g., magnetite) to magnetically 'hard' material (e.g., hematite or goethite). The S-ratio shows a persistent decrease with depth. If vertical soil mixing had occurred, then these two trends would have been obscured.

All measurements were collected on instrumentation at the Institute for Rock Magnetism at the University of Minnesota. The magnetic susceptibility of discrete samples was measured using an AGICO KLY-2 KappaBridge Susceptibility Bridge operating with a AC field of 300 A m^{-1} and a frequency of 920 Hz. Samples' natural remanent magnetizations were measured using a cryogenic rock magnetometer designed by 2G Enterprises. The S-ratio of each sample was determined using a ratio of isothermal remanent magnetizations, which were imparted using a Princeton Applied Research vibrating sample magnetometer. Samples' magnetizations were measured after exposure to a +1000 mT DC field and a -300 mT DC backfield. The S-ratio was calculated as:

$$S = \left| \frac{M_{-300\ mT}}{M_{1000\ mT}} \right|$$

Archaeological Data

Distribution of Diagnostic Artifacts—Block A

Fifty-two contiguous 1x1 m units were excavated at Block A. Artifacts recovered from the floodplain clays (A-Bss) show that the site was repeatedly occupied from before Clovis to the Late Prehistoric (Figs. S8 & S9). Diagnostic Late Prehistoric and Late Archaic period artifacts (*S37*), including 2 Perdiz, 1 Scallorn, 4 Ensor, 4 Edgewood, 1 Gary, 1 Darl, and 2 Castroville projectile points, occur from the surface to a depth of 91.10 m above datum (ad). Early Archaic artifacts, including 2 Wells and 4 Angostura projectile points, occur from 91.10 to 90.70 m ad. Paleoindian artifacts, including 2 Dalton, 6 Golondrina, and 2 Angostura projectile points occur from 90.70 to 90.475 m ad. Three Folsom points occur from 90.460 to 90.435 m ad (2.5 cm thick layer). Two of the three Folsom points were recovered 2.5 m apart separated vertically by only 1.1 cm. Clovis artifacts, including bifaces with overshot flaking, blades, and other tools occur between 90.425 and 90.40 m ad. Beneath the Clovis horizon lies the Buttermilk Creek Complex (90.40 to 90.20 m ad). The known-ages of time diagnostic artifacts ranging from Clovis to Angostura (90.40 – 90.95 m ad) correspond with the luminescence ages with which they are associated. A few Middle Archaic points occur in the late Holocene sediments (surface to 91.10 m ad), but these were likely curated by Late Archaic people. No younger diagnostics occur in the older levels with the exception of an Early Archaic Martindale point found in a sediment-filled burrow within the Clovis horizon.

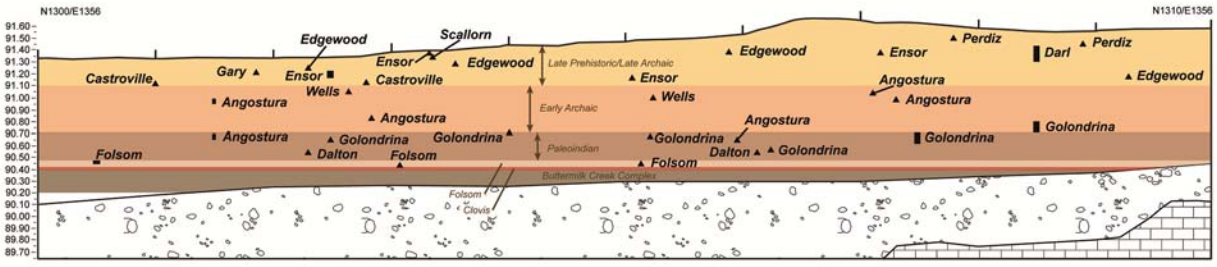

Figure S8. North to south cross-section of Block A showing the location of diagnostic projectile points.

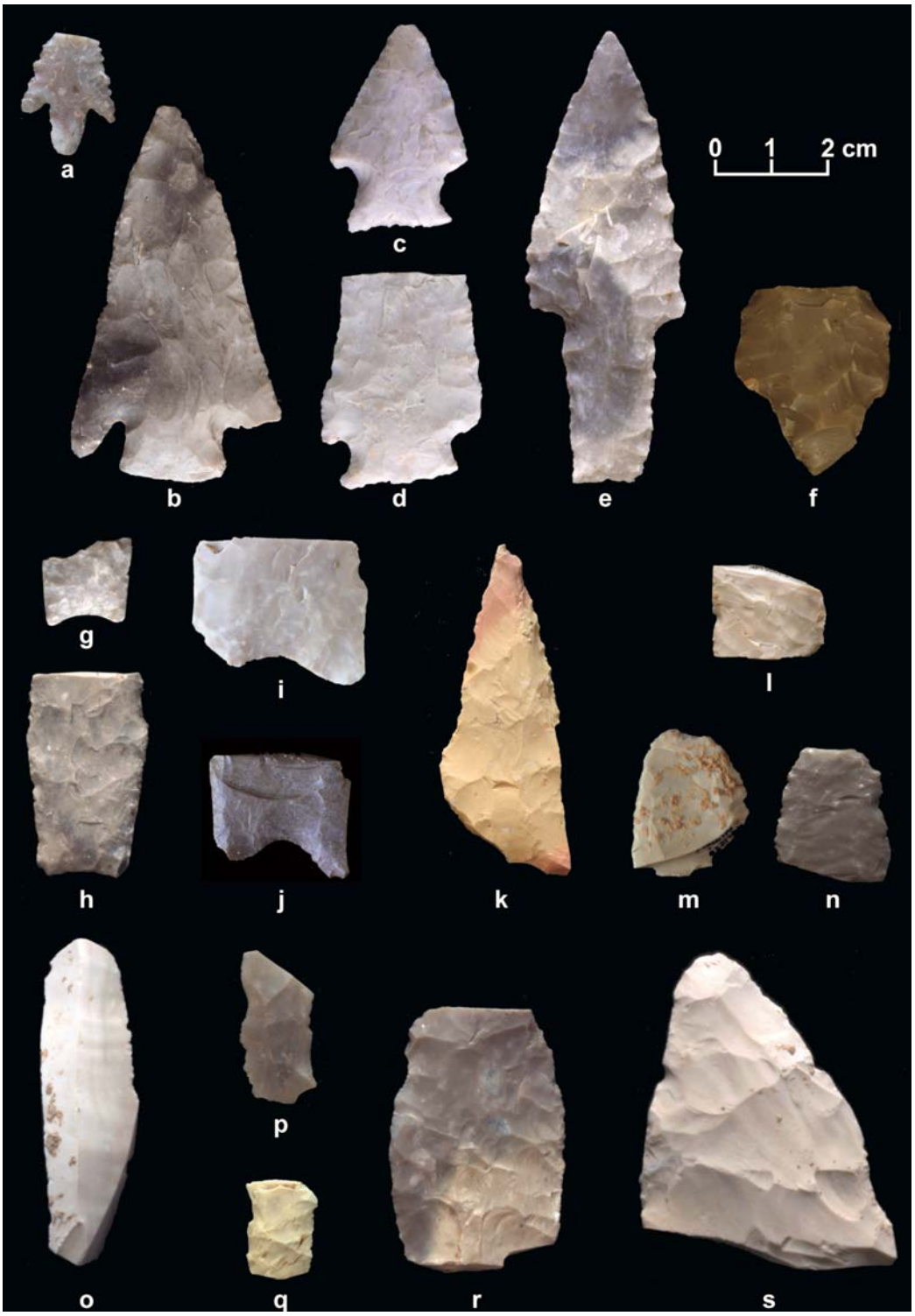

Figure S9. Diagnostic artifacts from Late Prehistoric, Archaic, and Paleoindian components. (a) Perdiz; (b) Castroville; (c) Edgewood; (d) Ensor; (e) Wells; (f) Gary; (g, h) Angostura; (i, j) Golondrina; (k) Dalton; (l, m, n) Folsom; (o) Clovis blade; (p, q) Clovis channel flakes; (r) late stage Clovis point preform midsection; (s) Clovis biface tip with overshot scars.

Clovis and Folsom Assemblages—Block A

The Folsom assemblage consists of 2319 artifacts, including two final stage fluted Folsom projectile point fragments broken during manufacture, one Folsom point tip that is fluted on one side and broke when the second flute attempt plunged (cf., *S38*), one large biface midsection, and one unifacial flake tool. The macrodebitage (n=571) is all late stage biface reduction debris. Of the size-class 5 and larger flakes with platforms (n=111), 41% are normal and 59% are biface thinning flakes. Four endthinning flakes were also recovered. The broken point fragments and the dearth of other tool types suggest this was a final stage Folsom point production locale.

The Clovis assemblage consists of 3374 artifacts, including eight late stage biface fragments, three unifacially edge-modified flake tools, five blade fragments, and one bladelet. Three late-stage biface fragments bear unretouched overshot scars, and one of these has an endthinning termination scar. Three bifaces are late-stage fragments, including a point preform tip and midsection. One biface is a projectile point ear fragment of a concave based point, and all worked edges of the ear are abraded. The three unifacial tools are all retouched flakes, and two are made on biface thinning flake blanks. The blades include two proximal fragments, each with two blade scars on the dorsal surface. One blade is a strongly curved midsection with two blade scars on the dorsal surface. The final two blades are medial fragments with three blade scars on the dorsal surface. Both appear to have been snapped. Microscopic analyses suggest some of these blade fragments may have been used. The bladelet is a proximal fragment with three parallel scars running down the dorsal surface. The macrodebitage (n=612) consists primarily of biface reduction products. Forty-three percent of the size-class 5 and larger flakes with platforms (n=256) in this level are normal and 55% are biface thinning flakes. No overshot flakes were recovered, but one non-cortical, distal partial-overshot fragment was recovered. Partial overshot flakes carry past the biface midline to the opposing edge, remove a thick portion of the flat edge, but do not fully wrap around to the opposite face. Partial-overshot flakes provide evidence of overface or past-the-midline flaking. While diagnostic Clovis blades were recovered, no evidence of on-site blade production (blade cores, core rejuvenation flakes) was found. Five endthining flakes, three of which are channel flakes, were also recovered. This tool assemblage, the late stage biface fragments, and the biface production debris suggests this was primarily a final stage Clovis point retooling site. The utilized flake tools may have been used on the organic components of Clovis technology.

Buttermilk Creek Complex Assemblage—Block A

The Buttermilk Creek Complex assemblage consists of 15,528 lithic artifacts including twelve bifaces, one discoidal core, twenty-three macroscopically edge-modified flake tools, five blade fragments, fourteen bladelets, and one piece of polished hematite. All are made of Edwards chert. Of the twelve bifaces, six are late-stage midsection and end fragments averaging 7.7 mm in thickness, and four are very small fragments. Flake scars on these fragments terminate at or before the midline.

One biface is lanceolate in shape and measures 59 mm in length, 6.7 mm in thickness, and may be a point preform fragment. The flaking on this piece is minimally invasive. This biface is burinated and the platform of this fracture remains on one end, but it is unclear whether this burination was purposeful or an accident of reduction. The other biface may be a chopper or adze-like tool. It is a large, thick secondary biface fragment that is 48 mm wide and 15.4 mm thick. The size of this piece suggests it is not part of a point preform reduction trajectory. It is plano-convex in cross-section with no cortex, and both faces have flake scars that carry past the midline. One face has multiple stacked step terminations around the tip and down both edges, but these do not appear to be thinning attempts.

A bifacially flaked discoidal flake core fragment measures 42 mm x 41 mm and is 14.5 mm thick. Flakes have been removed from all directions. The absence of a clear shaping or thinning strategy suggests it served as a flake core, and its small size suggests the core was discarded because it was exhausted. A core rejuvenation flake from a similarly sized discoidal core was also recovered.

Blade technology is present in the Buttermilk Creek Complex assemblage in the form of blades and bladelets. Five blade fragments were recovered, averaging 19.7 mm wide and 4.5 mm thick. The longest blade fragment (53.7 mm long) is a slightly curved midsection with a triangular cross-section and two dominant dorsal blade scars. Three are snapped blade midsections with triangular cross-sections and two dorsal scars. The other blade is a snapped midsection with three dorsal scars and a trapezoidal cross-section. Fourteen bladelet fragments were also recovered. Twelve of the fourteen bladelets have two dorsal blade scars and are triangular in cross-section. These average 11.8 mm wide and 3.2 mm thick. The remaining two possess three blade removal scars, are trapezoidal in cross-section, and average 14.4 mm wide and 4.3 mm thick. Microscopic analyses indicate that some of the blades and bladelets may have been used. No blade or bladelet cores were found, but two possible bladelet core fragments were recovered.

Evidence of macroscopic edge-modification occurred on 23 normal and biface thinning flake fragments and includes seventeen straight-to-concave edged tools, four notches, one graver, and two bifacially worked tools. The seventeen unifacial tools have retouch along the lateral flake margins or distal terminations to create straight or concave-edged tools. The intensity of retouch varies, with most exhibiting minimal flaking, but one more intensely worked side-scraper fragment was recovered. Four notches were recovered, with notch widths averaging 11 mm. One medial flake fragment has a shaped graver spur. One flake fragment is bifacially retouched and shaped. The bifacial flaking on this fragment served to shape the platform end of the flake blank and remove the bulb of percussion to thin the piece. These tools are generally small, with most (n=21) falling into debitage size classes 2 through 4.

The Buttermilk Creek Complex assemblage also contains a large number of bend and radially broken artifacts. Five of the biface fragments have radial breaks. One of these has radial breaks on three of the four sides and an apparent platform centered in the longest of these breaks, suggesting it was intentionally broken. This tool also has usewear evidence indicating the radial edges were used. The graver and one of the retouched flakes were resharpened along a fractured edge demonstrating that bend and radial break flakes also served as unifacial tool

blanks. Microscopic usewear analyses suggest that some additional radially broken or snapped flakes may have been expediently utilized without retouch.

In addition to the flaked tools, a polished piece of hematite was also recovered. The piece measures 31 mm x 22 mm x 17 mm and weighs 25.5 g. It is multifaceted with three primary worked surfaces. Linear striations that indicate multiple directions of use are clearly visible macroscopically on each surface.

Of the macrodebitage with platforms from the Buttermilk Creek Complex levels (*n*=843), 47% are normal and 51% are biface thinning flakes. The assemblage includes one distal overshot fragment and two partial-overshots. Eleven endthinning flakes were also recovered.

Tool and Debitage Counts—Block A

Artifacts from the Folsom, Clovis, and Buttermilk Creek Complex components were analyzed and classified into debitage and tool categories, and Table S8 presents these totals. Microdebitage (size class 6 [Table S15] and smaller) was counted. Macrodebitage (size class 5 and larger) was individually analyzed and classified into debitage subcategories (e.g. fragment, biface thinning flake, etc.). Following other blade technological studies (cf. *S39, S40*), blades and bladelets are distinguished based on size. Tools are divided into bifaces, edge modified tools, discoidal cores, and polished hematite. Table S9 presents artifact counts by excavation level. Folsom includes levels 31b and 32a, Clovis is level 32b, and Buttermilk Creek Complex is levels 33a-36b.

Table S8. Total debitage and tool counts from the Folsom, Clovis, and Buttermilk Creek Complex assemblages.

Class	Type	Folsom	Clovis	Buttermilk Creek Complex
Debitage[1]				
	Microdebitage total	1742[2]	2745	13204
	Macrodebitage total	571	612	2268
	Fragments and Shatter	182[2]	355	1425
	Normal Flakes	45[2]	110	399
	Biface Thinning Flakes	65[2]	141	433
	Endthinning Flakes	2[2]	5	10
	Discoidal Core Flakes			1
Tool				
	Blade		5	5
	Bladelet		1	14
	Biface			
	Point Preform	3	3	1
	Large Secondary	1		1
	Late-Stage Medial/End Fragments		5	6
	Small Fragments	1		4
	Discoidal Core			1
	Edge Modified Tool			
	Straight/Convex Edge	1	3	17
	Notch			4
	Graver			1
	Bifacially Shaped Flake			1
	Radial Break Tool[3]			
	Biface			1
	Straight Edge Modified			1
	Graver			1
	Polished Hematite			1
Total Artifacts		2319	3374	15528

[1] Microdebitage consists of size classes 6 and 7 artifacts. Macrodebitage consists of size class 5 and larger artifacts.
[2]These Folsom totals do not include counts from the 2008 field season.
[3] Radial Break Tool counts are included in the Biface and Edge Modified Tool counts.

Table S9. Tool and debitage counts by excavation level.

Level	Folsom Point	Point Preform	Late Stage Biface Fragment	Large Secondary Biface Fragment	Small Biface Fragment	Discoidal Core	Edge Modified Tool	Blade	Bladelet	Hematite	Overshot & Partial Overshot Flakes	Macrodebitage[1]	Microdebitage[1]
32a	3			1			1					571	1742
32b		3	5				3	5	1		1	612	2745
33a			1				1		3			500	2494
33b			1		1		3	3	2		1	455	2350
34a			1		1		3		2		1	406	2032
34b		1	1				6		1			313	1809
35a				1			2	1	3			206	1502
35b			1		1	1	3					159	1201
36a			1				1		1	1	1	136	1058
36b					1		4	1	2			93	758

[1] Microdebitage consists of size classes 6 and 7 artifacts. Macrodebitage consists of size class 5 and larger artifacts.
[2]The Folsom microdebitage total does not include counts from the 2008 field season.

Tool to Debitage Ratios—Block A

Comparing the number of tools (including blades and bladelets) to macrodebitage totals reveals important differences between the Folsom, Clovis, and Buttermilk Creek Complex assemblages (Table S10). There are significantly more tools in the Clovis and Buttermilk Creek Complex levels (p=0.028). This provides further evidence that artifacts within the Debra L. Friedkin site sediments are not being uniformly mixed, and demonstrates that Buttermilk Creek Complex inhabitants were using the site for a greater diversity of activities than Folsom and Clovis inhabitants.

Table S10. Folsom, Clovis, and Buttermilk Creek Complex tool counts compared to total macrodebitage. Tools include blades and bladelets.

Component		Type		
		Macrodebitage	Tools	*Total*
Folsom	Count	571	5	576
	Expected	563.4	12.6	576.0
Clovis	Count	612	17	634
	Expected	615.3	13.7	634.0
Buttermilk Creek Complex	Count	2268	55	2323
	Expected	2272.3	50.7	2323.0
Total	Count	3451	77	3528
		Likelihood Ratio chi-square		p = 0.028

Exploring Technological Continuity Between the Buttermilk Creek Complex, Clovis, and Folsom Assemblages

Here we compare the Folsom, Clovis, and Buttermilk Creek Complex assemblages to identify technological similarities and differences. For all three occupation periods, the Friedkin site served as an open campsite where only late stage reduction, tool resharpening, and camp related activities took place. While much is known of Folsom and Clovis lithic technological organization, we know nothing about the Buttermilk Creek Complex early or middle stage core reduction strategies. Because of this, the following comparisons must be regarded as preliminary.

Comparisons of the Folsom, Clovis, and Buttermilk Creek Complex assemblages reveal a number of similarities. All are late stage lithic reduction sites at which biface production was an important activity. Folsom, Clovis, and Buttermilk Creek Complex knappers used endthinning as a late-stage biface reduction technique. The Buttermilk Creek Complex preform fragment hints at lanceolate bifacial point production. The large flake removals on one Buttermilk Creek Complex biface suggests these knappers may have begun experimenting with overface or overshot reduction, a technique which later came to dominate Clovis biface reduction (*S40*). The

single Buttermilk Creek Complex overshot flake and the partial-overshot (or past-the-midline) flakes also show that Buttermilk Creek Complex biface flaking did carry past the midline in some instances. The radially broken or snapped biface and flake tools found in the Buttermilk Creek Complex assemblage resemble those documented elsewhere at Clovis (*S41*) and Folsom (*S42, S43*) sites. Finally, the Clovis (*S40*) and Buttermilk Creek Complex assemblages both show evidence of blade and bladelet technologies. Unfortunately, the technological production sequence of these removals is unknown because no definitive blade or bladelet core or core reduction debris has yet been recovered from the Debra L. Friedkin site. A large faceted piece of hematite from the Buttermilk Creek Complex layer is similar to those found at Folsom and Clovis sites.

Technological differences between these assemblages are also evident. No blades or bladelets were recovered from the Folsom assemblage. The discoidal core from the Buttermilk Creek Complex assemblage appears unique. Discoidal flake production in Clovis is suggested by a handful of flakes possibly from discoidal cores at the Aubrey site (*S41*), but the general absence of discoidal cores or debitage elsewhere suggests it was not a major Clovis reduction strategy. Discoidal reduction was, however, employed by Folsom groups, but this was a Levallois-style large flake removal technique that differs from that seen in the Buttermilk Creek Complex core (*S42, S44*). Finally, biface technologies also differ. Fluted bifaces and final flute/channel flakes have been recovered from the Folsom and Clovis components. No fluted bifaces or channel flakes have been recovered from the Buttermilk Creek Complex levels, which suggests that while endthinning occurred, Buttermilk Creek Complex knappers did not flute bifaces. Other than the one biface and the overshot/partial-overshot flakes, most Buttermilk Creek Complex bifaces show no evidence of past-the-midline flaking, suggesting this was not a dominant late stage thinning strategy.

Finally, comparison of the Folsom, Clovis, "late" Buttermilk Creek Complex (level 33a-34b), and "early" Buttermilk Creek Complex (level 35a-36b) complete flake assemblages reveals differences in two related platform traits, platform width (Table S11) and the frequency of platform isolation (Table S12). An analysis of variance test for platform width was significant ($p=0.007$), and post-hoc Bonferroni paired comparisons show that differences between Folsom and Clovis ($p=0.011$) are driving the ANOVA significance. Folsom platforms are significantly wider than Clovis platforms. The frequency of platform isolation also significantly differs ($p<0.001$). The Clovis component has the highest percentage of flakes with isolated platforms (23.0%), the Folsom and "late" Buttermilk Creek Complex components have fewer isolated platform flakes (17.8% and 19.1%), and the "early" Buttermilk Creek Complex component has the fewest (7.9%). The combination of these two traits shows that Clovis knappers were isolating platforms to control flake removals more than Folsom and Buttermilk Creek Complex knappers. Platform isolation appears to have increased through the Buttermilk Creek Complex components, peaked during Clovis, and decreased again during Folsom.

Table S11. Comparison of Mean Flake Platform Widths

Component	Mean Platform Width (mm)	Std. Deviation
Folsom	9.36	4.69
Clovis	7.76	3.46
"Late" Buttermilk Creek Complex	8.30	4.14
"Early" Buttermilk Creek Complex	8.80	5.00

Table S12. Comparison of Presence and Absence of Flake Platform Preparation.

Component		Platform Isolation		
		Absent	Present	*Total*
Folsom	Count	88	19	107
	Expected	88.1	18.9	107.0
Clovis	Count	181	54	235
	Expected	193.5	41.5	237.0
Buttermilk Creek Complex (late)	Count	471	111	582
	Expected	479.2	102.8	582.0
Buttermilk Creek Complex (early)	Count	197	17	214
	Expected	176.2	37.8	214.0
Total	Count	937	201	1138

Likelihood Ratio chi-square $p<0.001$

What do these similarities and differences tell us about the relationship of Buttermilk Creek Complex to later technologies? While the technological continuity between Buttermilk Creek Complex and Clovis cannot unequivocally be demonstrated until early and middle stage Buttermilk Creek Complex biface, blade, and informal reduction technologies are better understood, we see some important hints of technological links. Buttermilk Creek Complex knappers made and used bifaces, possibly made lanceolate points, endthinned bifaces, occasionally engaged in large bifacial flake removal resembling past-the-midline flaking, produced blades and bladelets, occasionally created and utilized radial or bend fractured tools, and utilized hematite. These technological features are similar to Clovis and later Paleoindian lithic industries and provide hints of technological continuity.

Beyond the Debra L. Friedkin site, the Aubrey Clovis site (*S41*), located in north-central Texas provides another opportunity to compare the Buttermilk Creek Complex assemblage to an open Clovis campsite. In terms of artifact types and counts, the composition of the Aubrey assemblage is remarkably similar to the Friedkin Buttermilk Creek Complex assemblage (Table S13). At both sites, bifacial reduction debris comprises much of the assemblage, but few bifaces and no complete points were recovered. Normal flakes were also produced in large quantities. While both sites yielded a handful of blades and bladelets, there is little evidence of on-site blade production (Aubrey yielded a single small core tablet flake—from which bladelets were removed). Finally, the tool assemblages at both sites are dominated by unifacial tools, and these tools are similar in many ways, but important differences are also evident. The Aubrey unifacial tool assemblage is more diverse and (Table S14) includes all tool types macroscopically

identified in the Buttermilk Creek Complex assemblage, including sidescrapers, gravers, notches, retouched flakes, retouched radial/bend fractured fragments, a chopper, and a polisher. Aubrey has more types of scrapers and also has multiple tools (e.g. end scraper with a graver spur) which are absent in Buttermilk Creek Complex, reflecting a more heavily curated and recycled assemblage. One significant difference between the Aubrey and Buttermilk Creek Complex assemblages lies in the blanks selected for tool use. Eleven of the Aubrey tools are made on blades; however, no Buttermilk Creek Complex tools with macroscopic retouch are on blades. This suggests a key difference in the relative importance of blade technology to large flake tool production. Overall, the Aubrey and Buttermilk Creek Complex debitage and tool assemblages are remarkably similar, suggesting the same kinds of activities were taking place at both campsites, and again showing that similar stone tool technologies were being employed.

Table S13. Artifact Counts From the Aubrey Site (after *S41*:Table 9.1).

Artifact Type	Count
Debitage	
Chips-chip fragments	7804
Flakes-flake fragments	1069
Biface thinning flakes	422
Core trimming elements	11
Blades	1[a]
Bladelets	29
Uniface resharpening chips	440
Cores	1
Tools	
Bifacial	4
Unifacial	60
Total	9841

a. 11 blades were made into tools and are included in the unifacial tool category.

Table S14. Aubrey Unifacial Tool Assemblage (after *S41*:Table 9.11).

Tool Type	Count
End Scraper	5
Other Scraper	5
Knife	1
Retouched Flake	21
Notch/denticulate	1
Graver/Bec	5
Chopper	1
Radial/Bend Fractured tool	15
Abrader/polisher	1
Multiple tool	5
Total	60

Site Formation—Distribution of Lithic Artifacts and Calcium Carbonate Accumulations—Block A

During excavation, the sediment-filled vertic cracks were identified and mapped at the base of each level (*S45*). These cracks diminished in width from 15 mm at the surface to 1-2 mm at level 34 (*S45*). Artifacts at all levels were found in the areas between the sediment-filled cracks and not within them. Field observations and soil micromorphological studies show that chert flakes occur between and within peds. An analysis of artifact size distribution with depth within one 1 m^2 excavation unit from the 2009 season shows that there is no sorting of artifacts by size from the surface through level 36b (i.e., the ratio of large to small artifacts remains constant with depth), confirming that there is no vertical mixing of artifacts.

The old model of pedoturbation within Vertisols (*S46, S47*) predicted that vertic movement caused large clasts to move upward as they were differentially heaved and smaller clasts would move downward as they fell down seasonally open cracks. According to this model, argilliturbation processes would vertically size-sort artifacts within the Vertisol. Thus, deeper levels should have more small-size artifacts compared to large-size artifacts and upper levels should have more large-size artifacts compared to small-size artifacts.

Even though Vertisols are no longer considered to be mixed (*S35*), the artifact size distribution for excavation unit N1305 E1361 was analyzed to determine if any size sorting had taken place. This unit was excavated in 2.5 cm levels from the surface down to culturally sterile sediment with all sediment water-screened through 1/8" mesh. A total of 13,458 artifacts collected from this unit were size-sorted into 7 categories using a series of geologic screens (Table S15).

Artifact quantities for each size category with depth are shown in Figure S10. Artifact quantities remain above 50 through level 36b and decrease rapidly below this depth. Figure S11 shows how these artifacts vary in size with depth. This graph shows that the proportion of artifact size categories remains relatively constant from Level 16b to Level 36b. The fluctuations at the surface (Levels 15b and 16a; 0-5 cm below the surface) are the result of partial levels and excavation of disturbed sediments. A study of all artifacts recovered from 4 m^2 in 2007 and from two 0.5 x 0.5 m^2 units from the 2008 season, shows the same trends—no artifact size sorting with depth (*S45*).

In addition, the presence and absence of calcium carbonate accumulations on size 1-5 artifacts and macrodebitage was noted for each level (*S45*) for the 2007, 2008, and 2009 samples. Analyses consistently show that calcium carbonate coatings do not occur on artifacts from the surface through level 24. Artifacts first show calcium carbonate accumulations starting in level 25 and the number of artifacts with calcium carbonate accumulation increases with depth. Almost 90% of the size 1-5 artifacts and macrodebitage in the Buttermilk Creek Complex levels have calcium carbonate accumulations. The presence and absence of calcium carbonate on artifacts and the increase in calcium carbonate accumulations on artifacts in the Paleoindian and Buttermilk Creek Complex levels tracks the changing concentrations of pedogenic calcium carbonate in the soil. This again, shows that artifacts are not drifting downward through the

floodplain deposits. These findings support the pedologic analyses and the modern interpretation of Vertisol formation in which the soil matrix is not mixed (*S35*).

Table S15. Lithic Artifact Size Categories.

Artifact Size Class	Screen Size	
1	>3.75 cm	(>1 1/2")
2	2.5-3.75 cm	(1-1 1/2")
3	1.875-2.5 cm	(3/4-1")
4	1.25-1.875 cm	(1/2-3/4")
5	0.95-1.25 cm	(3/8-1/2")
6	0.625-0.95 cm	(1/4-3/8")
7	0.335-0.625 cm	(1/8-1/4")

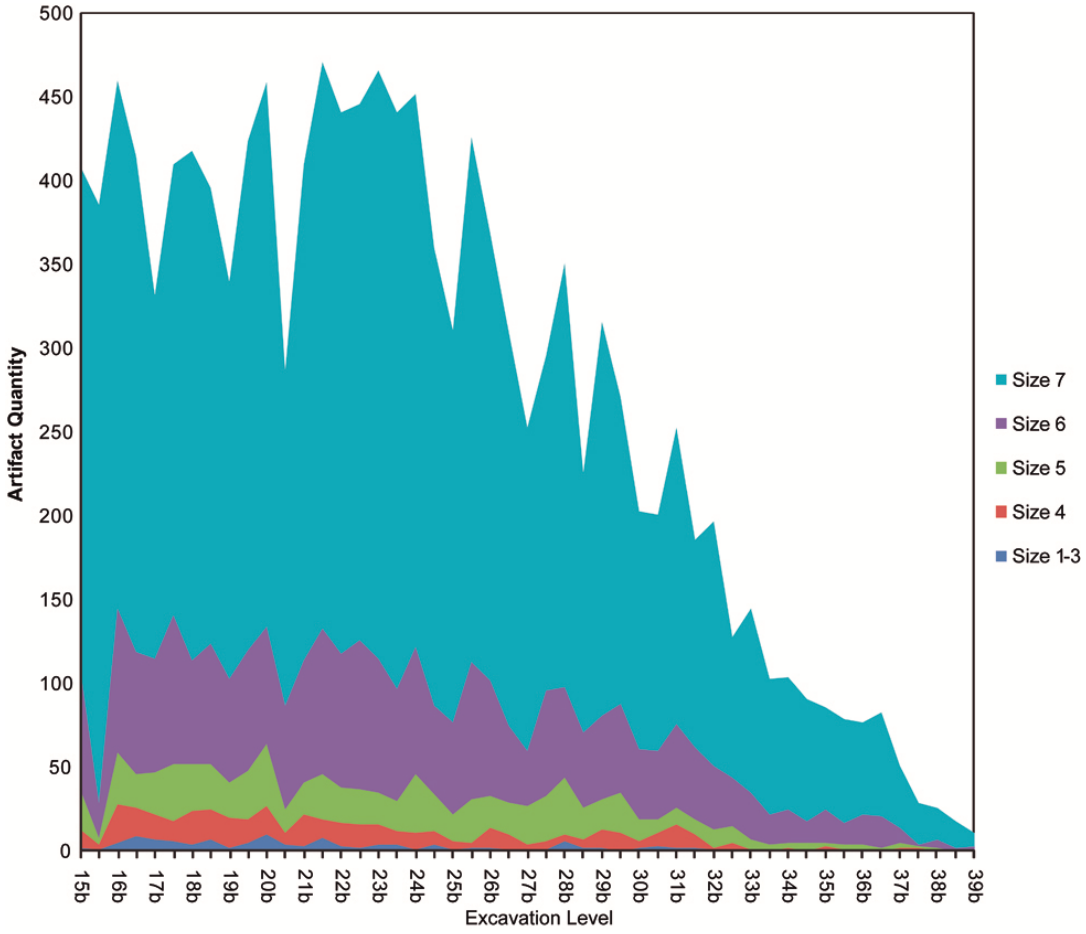

Figure S10. Total number of artifacts by level in excavation unit N1305 E1361.

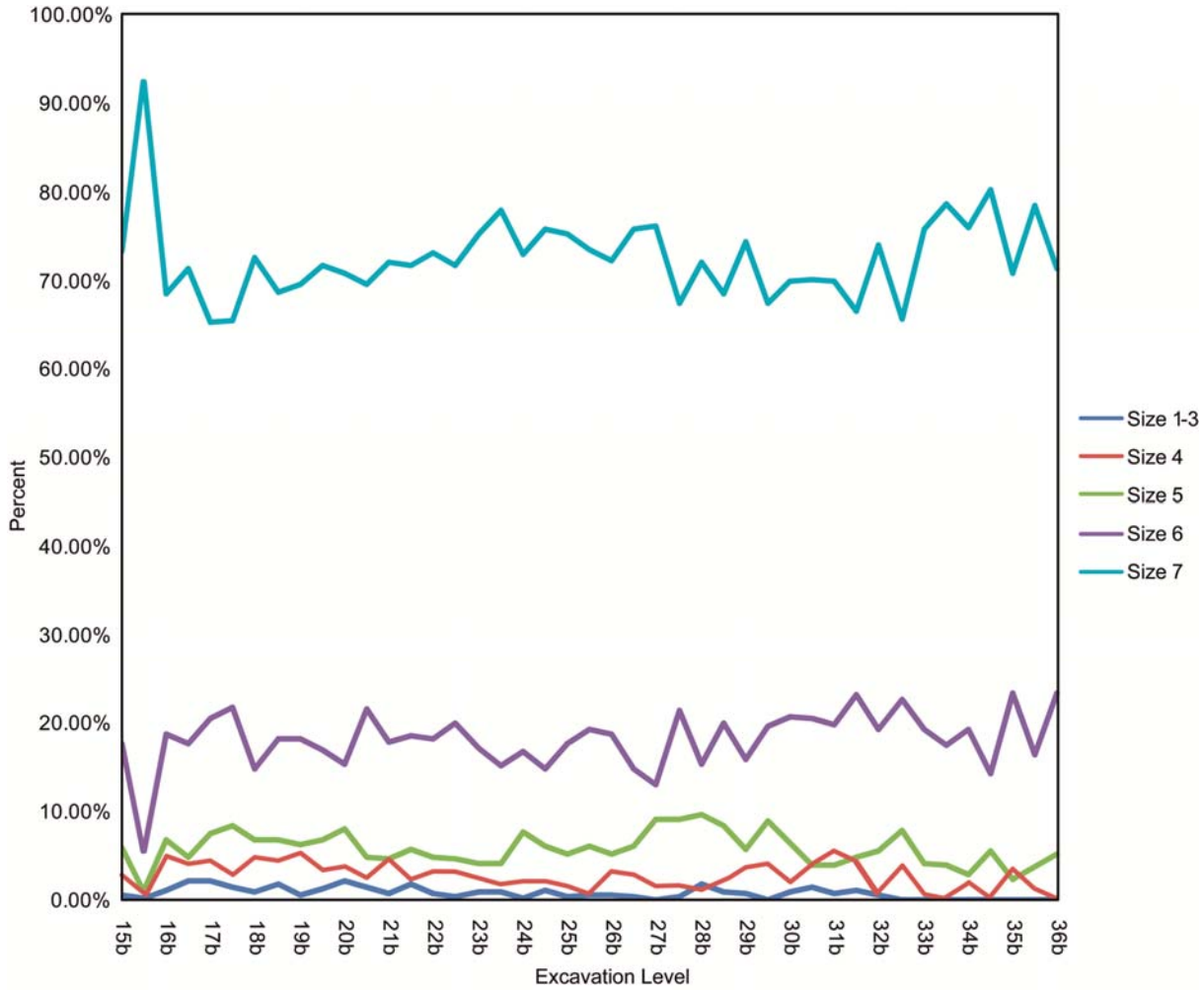

Figure S11. Variation in artifact size with depth in excavation unit N1305 E1361.

Refit Studies

While no comprehensive, systematic refitting study of the entire assemblage has yet been conducted, preliminary analyses demonstrate that refits are present, and they occur within and above the Buttermilk Creek Complex levels. Thus far, five refits have been identified (Table S16) including two technological refits and three conjoining refit flake fragments (cf. *S48*). All refits were found within the same level of the same unit, and therefore each refit group has a maximum vertical separation of 2.5 cm and maximum horizontal separation of 1.41 m. For the refits of which both artifacts were piece-plotted (Refit Groups 3 and 4) vertical and horizontal distances were significantly smaller. The identification of closely spaced technological refits provides further evidence that artifacts are not significantly moving horizontally or vertically within the Friedkin site matrix. In addition, both fragments of Refit Group 4 have calcium carbonate accumulations on the break surface, suggesting that the flake fragmentation occurred during the reduction process.

It is worth mentioning again that diagnostic artifacts were in many cases found within a thin stratigraphic interval. For example, two Late Archaic Castroville projectile points were found within 2 cm vertical distance from one another over a 2.5 m horizontal distance. All Folsom points were found within a 2.5 cm thick layer and two of these points were separated vertically by only 1.1 cm.

Table S16. Artifact refit groups.

Refit Group	Artifact	Level	Northing	Easting	Elevation	Refit Type	Horizontal distance	Vertical distance
1	2855-6	27b	1305.43	1355.58		Technological	0.04 cm	0-2.5 cm
	2855-7	27b	1305.47	1355.58				
2	4797	34a	1305*	1359*		Conjoin	0-1.414 m	0-2.5 cm
	4797	34a	1305*	1359*				
3	4777-1	34b	1302.5	1357.795	90.42	Conjoin	0.0	0.69 cm
	4777-4	34b	1302.5	1357.795	90.351			
4	4817-4	34b	1301.89	1358.57	90.347	Conjoin	0.29 cm	.06 cm
	4817-5	34b	1301.875	1358.585	90.353			
5	4861-1	34b	1304.51	1359.1	90.355	Technological	0-1.034 m	0.18 cm
	4861	34b	1304*	1359*				

* Artifacts found in the screen and not piece-plotted.

Preliminary Usewear Analysis

A preliminary usewear study was conducted on artifacts from the Buttermilk Creek Complex levels. A Leica DMLA compound microscope fitted with Nomarski optics was used to observe usewear characteristics at magnifications of 100X, 200X, and 500X. Images were recorded with a CoolSnapPro camera integrated with Image-Pro Plus software in order to produce a clear focused image at high magnification. Artifacts were cleaned with a mild detergent and sonification. Alcohol on a cotton swab was used to periodically to remove oils and grease from handling.

Artifact 4867 (Fig. S12) is a bladelet with a triangular cross-section. Both lateral edges of the bladelet exhibit flaking from use that alternates between the dorsal and ventral surfaces along almost its entire length. The flake removals occur at two scales. Macro-flakes scars (produced unintentionally during use) exhibit both feather and step terminations; the most invasive of which are approximately 0.8 mm from the edge. Micro-flake scars are also present along both edges and have feather, step, and 'half-moon' terminations (*S49*). Polish and linear indicators that trend parallel to the edge of the bladelet occur on both the dorsal and ventral surfaces along most of the entire length of the bladelet. This use-wear is confined to the margins of the flake scars (Fig. S11, point 2), arrises between flake scars, and other high points such as hackles (Fig. S12, point 1). The location and regularity of these characteristics indicate that this bladelet was likely used as a cutting tool on both edges.

Artifact 6171-1 (Fig. S13) is a blade with a triangular cross-section and alternately flaked edges. Both macro- and micro-flake scars produced during use are present along the entire

length of both edges of the blade and exhibit feather, step, and 'half-moon' terminations. Maximum invasiveness of the macro-flake scar terminations is approximately 3.0 mm. Usewear in the form of polish and linear indicators occur along the length of both edges but is confined to high points such as flake scar margins (Fig. S13, points 3, 5), arrises between adjacent flake scars (Fig. S13, point 2), and hackles (Fig. S13, point 4). The location, direction, and appearance of polish and linear indicators parallel to the edge suggests that this blade was used as a cutting or scoring tool on a relatively hard material such as bone. The point produced by the snap fracture at the distal end exhibits extensive wear in the form of polish and striations (Figs. S13, point 1). The striae are oriented parallel to the long axis of the blade, indicating grooving or incising of a fairly hard material.

Artifact 4819-3 (Fig. S14) has four snapped edges and one unifacially notched edge. The three points formed by the intersection of the snapped edges have extensive polish and striae (Fig. S14, points 1, 2, 3). The same wear also occurs on the edges of the snap fractures, but is less pronounced in comparison to the tips. The direction of this wear in some places is transverse to the edge and in other places is parallel to the edge. This wear pattern indicates this tool was used to incise a hard material such as bone and wood. The notch as evidence of wear: step fractures likely created by scraping a hard material. The edges of the step fractures exhibit polish.

Artifact 5965-2 (Fig. S14) is a biface that was radially broken, leaving it with four adjacent snapped edges and one bifacial edge. Usewear in the form of polish and striae occur on the snapped edges (Fig. S14, point 6). Polish and striae are very prominent at the points where the broken edges intersect (Fig. S14, points 4, 5). The polish and striae indicate that these points and snapped edges were used on a hard material. Because the polish is invasive and the orientation of the striae is oblique to the point, this tool was likely used for incising a groove into a hard material such as bone, antler, or wood. The biface edge shows polish and linear indicators trending parallel and transverse to the edge that is indicative of cutting and scraping (Fig. S14, point 7).

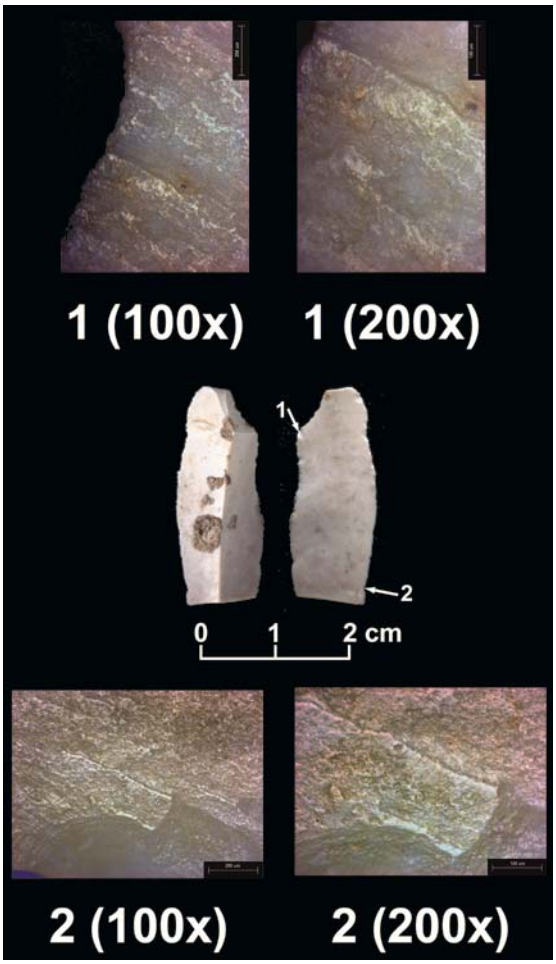

Figure S12. Bladelet with microscopic usewear. (100X, scale 200 microns; 200X, scale 100 microns).

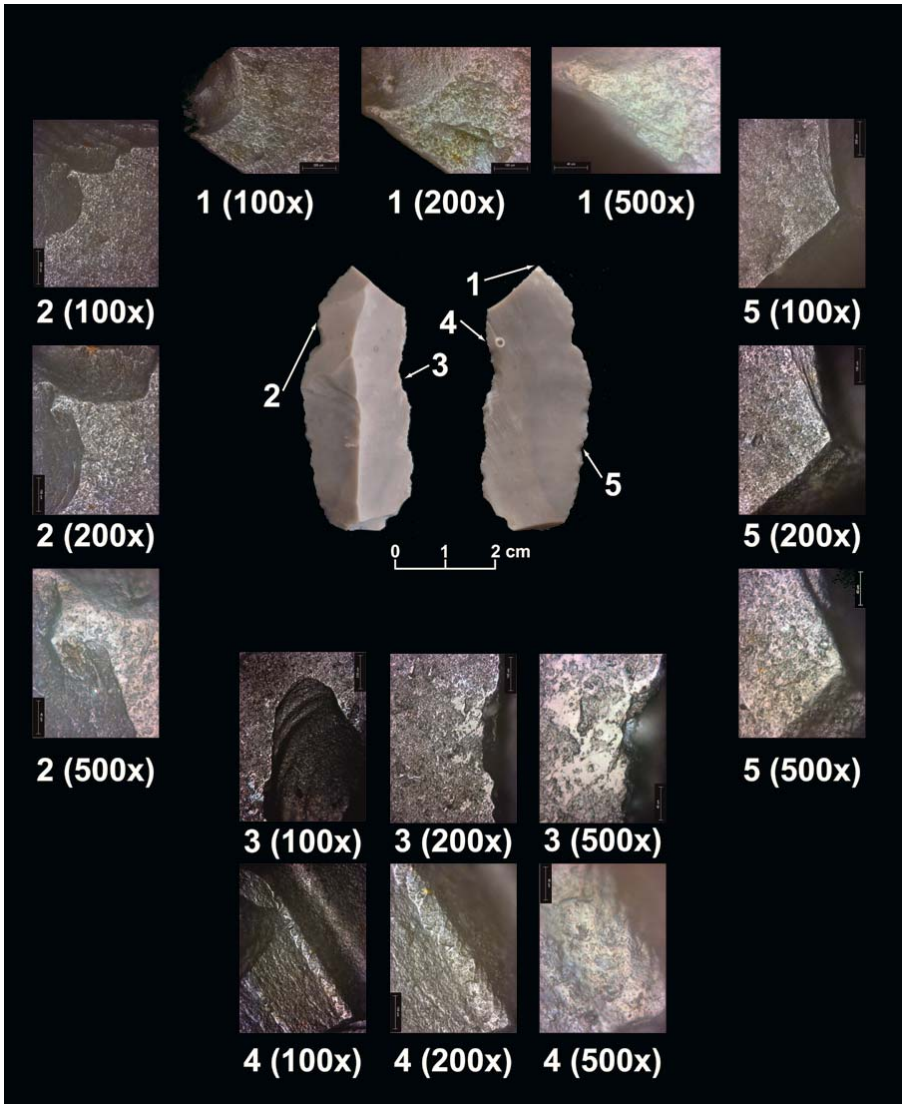

Figure S13. Blade with microscopic usewear. (100X, scale 200 microns; 200X, scale 100 microns; 500X, scale 40 microns).

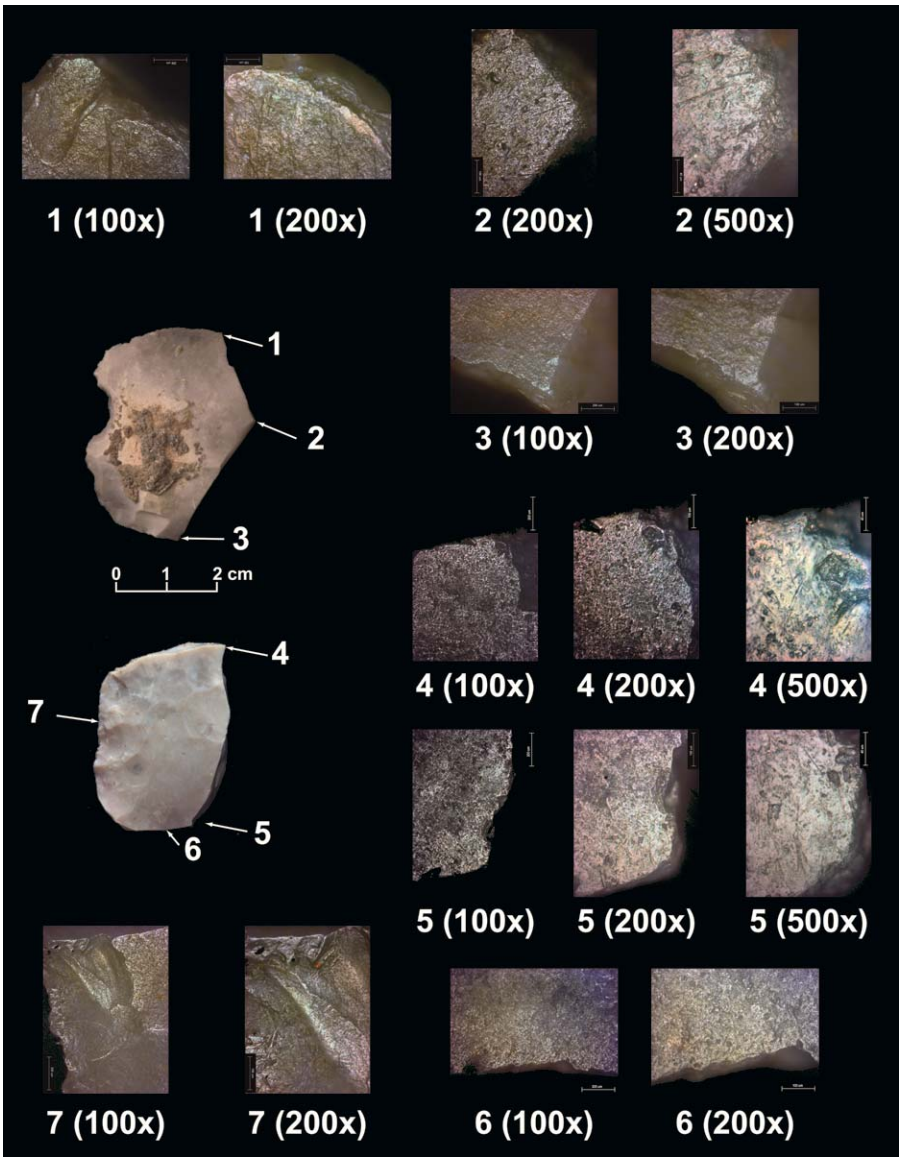

Figure S14. Edge-modified tool (notch with radial/bend breaks) and biface with radial breaks showing microscopic usewear. (100X, scale 200 microns; 200X, scale 100 microns; 500X, scale 40 microns).

References

S37. M. B. Collins, in *The Prehistory of Texas*, T. K. Perttula, Ed. (Texas A&M University Press, 2004), pp. 101-126.

S38. F. Sellet, *J. Archaeol. Sci.* **31**, 1553-1566 (2004).

S39. K. E. Graf, *J. Archaeol. Sci.* **37**, 210-233 (2010).

S40. B. A. Bradley, M. B. Collins, A. Hemmings, *Clovis Technology* (International Monographs in Prehistory, Ann Arbor, 2010).

S41. R. Ferring, *The Archaeology and Paleoecology of the Aubrey Clovis Sites (41DN479) Denton County, Texas* (Center for Environmental Archaeology, University of North Texas, Denton, 2001).

S42. T. A. Surovell, *Toward a Behavioral Ecology of Lithic Technology: Cases From Paleoindian Archaeology* (University of Arizona Press, Tucson, 2009).

S43. M. J. Root, in *Archaeology of the Bobtail Wolf Site (32DU955a): 1993-1994 Progress Report*, M. Root, A. Emerson, Eds. (Center for Northwest Archaeology, Washington State University, Pullman, 1994), pp. 147-190.

S44. G. C. Frison, B. A. Bradley, *Folsom Tools and Technology at the Hanson Site* (Academic Press, New York, 1980).

S45. J. L. Keene, *Site Formation Processes at the Buttermilk Creek Site (41BL1239), Bell County, Texas* (Thesis, Texas A&M University, College Station, 2009).

S46. D. H. Yaalon, D. Kalmar, *Earth Surf. Proc*. **3**, 31 (1978).

S47. W. R. Wood, D. L. Johnson, in *Advances in Archaeological Method and Theory, volume 1*, M. B. Schiffer, Ed. (Academic Press, New York, 1978), pp. 315-381.

S48. J. P. Laughlin, R. L. Kelly, *J. Archaeol. Sci.* **37,** 427-433 (2010).

S49. L. Keeley, *Experimental Determination of Stone Tool Uses: A Microwear Analysis* (University of Chicago Press, Chicago, 1980).